University of the Aegean

School of Engineering

Department of Financial Engineering and Management

Master by Research Dissertation Thesis

‘Effect of the concentration of carbon-based nanostructures as reinforcement to the mechanical properties of cement-based materials‘

Dipl. Ing. Anastopoulos Stylianos

Chios, September 2021

ABSTRACT

In recent years, composites have been successfully strengthened at micrometer scale using different types of reinforcements. Production of carbon nanotubes and of graphene enabled the reinforcement of cement-based materials at the nano-scale. The produced nanocomposites have greatly increased the mechanical properties, especially the “effective” properties such as modulus of elasticity and Poisson ratio. With their widespread exploitation a need has emerged, the ability to simulate and predict the mechanical properties and consequently the mechanical behavior of cement-based composite materials according to type, geometry and volume fraction of inclusions used. Another important need is the ability to identify the optimum material synthesis of a composite that will fill the intended needs in the most economically efficient way when different types of inclusions are in the engineer’s disposal; and even so when more than one type of inclusion may be used in conjunction with the cement matrix.

Therefore, the main scope of this Thesis was the development of a methodology for the calculation of the mechanical properties of a cement-based nano-reinforced composite and to predict by extrapolation the properties of any composite with the same matrix and inclusions, but with varying inclusion volume fractions. Research in international literature was initially conducted for the available methods of homogenization and experimental data of cement-based matrix reinforced with multi-walled carbon nanotubes (MWCNTs) were retrieved from literature data. The selected homogenization methods were the multi-step method and the finite element method. Inclusion orientation was simulated with two different methods: the fixed angles and the random orientation method. The homogenization tool of the ANSA® software package was exploited for the modeling of the inclusion geometries in a cubic matrix and for mesh generation. A Representative Volume Element (RVE) was constructed with either random orientation tensor algorithm or periodic geometry algorithm tools and for different concentrations of the nano-reinforcement. Finite element modelling of the pre-cracked specimens for 4 point bending flexural tests followed, and the simulation results of the crack mouth opening displacement (CMOD) were compared against the experimental results, in order

to identify the most accurate composition. Effective modulus of elasticity was expressed as a correlation of inclusion volume fraction (v_f).

Secondarily, the synthesis optimization problem was addressed. A methodology was developed in order to achieve optimal material synthesis with a target valued for the effective modulus of elasticity. The Interior Point Optimization (IPOpt) algorithm was used to guide the iterations applied to the homogenized material properties simulated. Three study cases were investigated in order to validate the proof of concept.

ΠΕΡΙΛΗΨΗ

Τα τελευταία χρόνια τα σύνθετα υλικά έχουν επιτυχώς ενισχυθεί στην κλίμακα του μικρομέτρου χρησιμοποιώντας διαφορετικούς τύπους ενίσχυσης. Η παραγωγή νανοσωλήνων άνθρακα και γραφενίου επέτρεψε την ενίσχυση υλικών με βάση το τσιμέντο στη νανο-κλίμακα. Τα νανοενισχυμένα δομικά υλικά έχουν αυξημένες μηχανικές ιδιότητες, ιδιαίτερα ισοδύναμες (effective) ιδιότητες όπως το μέτρο ελαστικότητας και ο λόγος Poisson. Με την ευρεία χρήση των νανουλικών, προέκυψε η ανάγκη της προσομοίωσης και πρόβλεψης των μηχανικών ιδιοτήτων και της συμπεριφοράς ενός σύνθετου υλικού με βάση το τσιμέντο σύμφωνα με τον τύπο, τη γεωμετρία και το κλάσμα όγκου των πρόσθετων που χρησιμοποιούνται για την ενίσχυση. Μια άλλη σημαντική ανάγκη είναι η ικανότητα προσδιορισμού της βέλτιστης σύνθεσης του υλικού που θα καλύψει τις προβλεπόμενες ανάγκες με τον πιο οικονομικά αποδοτικό τρόπο, όταν διαφορετικοί τύποι πρόσθετων είναι στη διάθεση του μηχανικού, ακόμη και όταν μπορούν να χρησιμοποιηθούν περισσότεροι από ένας τύποι πρόσθετων σε συνδυασμό με τη μήτρα τσιμέντου.

Ως εκ τούτου, το κύριο πεδίο αυτής της ερευνητικής εργασίας ήταν να αναπτυχθεί μια μεθοδολογία για τον υπολογισμό των μηχανικών ιδιοτήτων ενός σύνθετου με βάση το τσιμέντο και να προβλέψει αναγωγικά τις μηχανικές ιδιότητες οποιουδήποτε σύνθετου με την ίδια μήτρα και πρόσθετα, αλλά με ποικίλα κλάσματα όγκου πρόσθετων. Η έρευνα στη διεθνή βιβλιογραφία διεξήχθη αρχικά για να επιλεχθούν απο τις διαθέσιμες μεθόδους ομογενοποίησης και ανευρέθηκαν πειραματικά δεδομένα μήτρας με βάση τσιμέντο ενισχυμένα με νανοσωλήνες άνθρακα πολλαπλών τοιχωμάτων (MWCNT). Οι μέθοδοι ομογενοποίησης που επιλέχθηκαν ήταν η μέθοδος πολλαπλών σταδίων (multi-step) και η μέθοδος πεπερασμένων στοιχείων. Ο προσανατολισμός των πρόσθετων προσομοιώθηκε με δύο διαφορετικές μεθόδους: με σταθερές γωνίες και με την μέθοδο τυχαίου προσανατολισμού (random orientation). Το εργαλείο ομογενοποίησης του πακέτου λογισμικού ANSA® αξιοποιήθηκε για τη μοντελοποίηση των γεωμετριών των νανοϊνών σε μία κυβικής γεωμετρίας μήτρα και για τη δημιουργία πλέγματος. Ένα αντιπροσωπευτικό στοιχείο όγκου (random volume element) κατασκευάστηκε είτε με τον τανυστή τυχαίου προσανατολισμού είτε με εργαλεία αλγορίθμων περιοδικής γεωμετρίας και για διαφορετικές συγκεντρώσεις του νανο-

οπλισμού. Ακολούθησε μοντελοποίηση πεπερασμένων στοιχείων των προ-ρηγματωμένων δοκιμίων για δοκιμές κάμψης 3 σημείων και τα αποτελέσματα προσομοίωσης της μετατόπισης του ανοίγματος του άκρου της ρωγμής συγκρίθηκαν με τα πειραματικά αποτελέσματα, προκειμένου να προσδιοριστεί η πιο ακριβής σύνθεση. Το ισοδύναμο (*effective*) μέτρο ελαστικότητας εκφράστηκε ως συσχέτιση του κλάσματος όγκου πρόσθετων (v_f).

Δεύτερον, αντιμετωπίστηκε το πρόβλημα εύρεσης της βέλτιστης σύνθεσης. Αναπτύχθηκε μια μεθοδολογία προκειμένου να επιτευχθεί η βέλτιστη σύνθεση υλικού για μία τιμή στόχο του μέτρου ελαστικότητας. Ο αλγόριθμος βελτιστοποίησης εσωτερικών σημείων (Interior Point Optimization) χρησιμοποιήθηκε για να οδηγήσει τις επαναλήψεις που εφαρμόστηκαν με δεδομένες τις προσομοιωμένες ιδιότητες του ομογενοποιημένου υλικού. Τρεις περιπτώσεις μελέτης δοκιμάστηκαν για την απόδειξη της έννοιας και τον προσδιορισμό επαρκούς αριθμού επαναλήψεων.

Table of Contents

List of Figures

1. Introduction

1.1 Reinforcing materials

Reinforcing a material adds rigidity and greatly impedes crack propagation. In essence, the mechanical properties of the matrix are enforced, resulting in most cases in stiffer, stronger and harder material than the original matrix. The type of reinforcement can help distinguish the composite in four basic categories: particulates, fibers, flakes and fillers, e.g. (1).

1.1.1 Flakes

These are reinforcing materials existing in flat platelet form and having approximately two-dimensional geometry with strength and stiffness in two directions. With their suspension in glass or plastic an effective composite material can be formed. Commonly, flakes are packed parallel to one another, meaning that in comparison with fiber reinforced materials, flakes can provide a higher density. Some of these flake materials are mica, aluminum, and silver (Figure 1). When mica flakes are embedded in a glassy matrix, the resulting composites can be machined with ease and as such are used widely in electrical applications. Flakes of aluminium in paints and coatings in general orient themselves in parallel. Where there is need for a good conductor, flakes of silver are an option (1).

Figure 1 Photograph showing silver mica flakes (2)

1.1.2 Fillers

Powders and particles inserted into a matrix in order to enhance its physical and mechanical properties are called fillers. Fillers are also helpful in lowering the percentage used of a more expensive binder material. Thermal conductivity, electrical resistivity, friction, wear resistance, and flame resistance can all be enhanced using fillers. Some typical examples of fillers are calcium carbonate, aluminum oxide, lime (also known as calcium oxide), fumed silica, treated clays, and hollow glass beads (1).

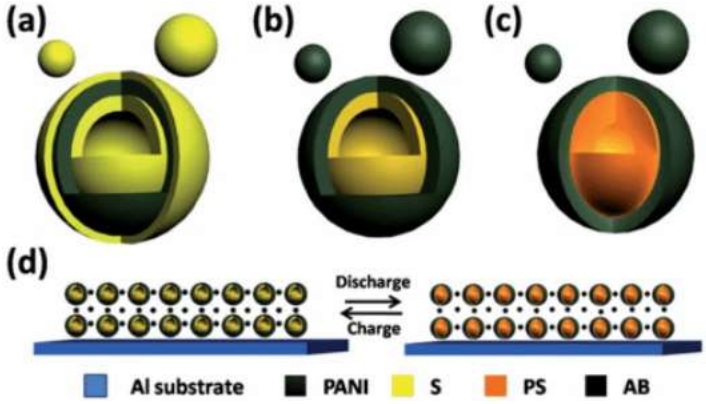

Figure 2 Schematic illustration of the hollow sphere PANI/S composite during the charge/discharge process. (a) The initial PANI-S composite, (b) the cycled PANI-S composite, (c) the lithiated PANI-S Composite and (d) the schematic illustration of integrity of the hollow PANI-S cathode with severe Volume change during charge/discharge (3)

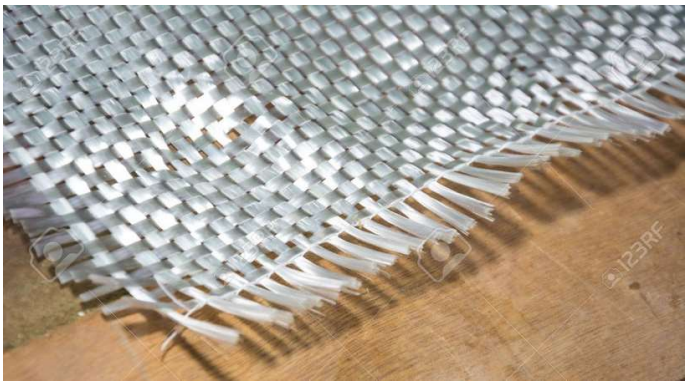

Figure 3 White glass fiber composite raw material background (4)

1.1.3 Fibers

Fibers are ropes or strings with a substantial aspect ratio (> 100) used as a component in composite materials. Fiber cross-sections can be of a circular, square or hexagonal form. Fibers usually used are glass fibers (Figure 4), which consist primarily of silicon dioxide and metallic oxide modifying elements and are generally produced by mechanical drawing of molten glass through a small orifice. These have the benefits of a very low cost simultaneously providing high corrosion resistance. Typical uses include fishing rods, storage tanks, and aircraft parts; 2) aramid fibers, which have higher specific strength while lighter than glass and more ductile than carbon. Examples of industrial application are armor, protective clothing, and sporting goods; 3) carbon fibers (Figure 4), can be made from an oxidized polyacrylonitrile or via pyrolysis carbonized polymers. Carbon fibers may offer more than 950 GPa with low density. Their diameter usually falls somewhere in the range between 5 and 8 μm, 4) boron fibers, with characteristics such as high stiffness and compressive strength, and relatively large diameters (0.05–0.2 mm). Such boron fiber composites have been utilized in aerospace structures where stiffness is of essence. 5) silicon carbide fibers, for high-temperature metal and ceramic matrix composites (CMC) because of excellent oxidation resistance, high modulus, and strength in high-temperature atmosphere (1).

Figure 4 Carbon fiber and aramid fiber (5)

1.2 Reinforced concrete history

François Coignet was the first to use iron-reinforced concrete as a technique for constructing building structures (6). In 1853, Coignet built the first iron reinforced concrete structure, a four-story house at 72 rue Charles Michels in the suburbs of Paris, which still stands as seen in Figure 5. Coignet's descriptions of reinforcing concrete suggests that he did not do it for means of adding strength to the concrete but for keeping walls in monolithic construction from overturning (7). In 1854, English builder William B. Wilkinson reinforced the concrete roof and floors in the two-story house he was constructing. His positioning of the reinforcement demonstrated that, unlike his predecessors, he had knowledge of tensile stresses, e.g. (8), (9) and (10).

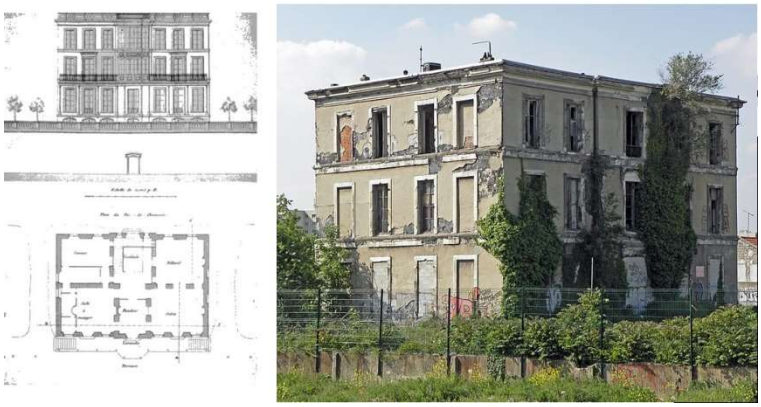

Figure 5 The world's first iron-reinforced concrete structure, a four-story house at 72 rue Charles Michels (6)

Joseph Monier, a 19th century French gardener, was a pioneer in the development of structural, prefabricated and reinforced concrete, having been dissatisfied with the existing materials available for making durable flowerpots (11). Monier filed and was granted the patent for reinforcing concrete flowerpots by means of mixing a wire mesh and a mortar shell. Even further, in 1877, Monier was issued another patent for a more advanced technique of reinforcing concrete columns and girders, using iron rods placed in a grid pattern. It is in doubt whether Monier understood the mechanical properties and concepts such as tensile stresses in design (Figure 6) (12).

Figure 6 In 1873 Monier applied for an addition to patent 77165 to cover bridges, and in 1875 built his first bridge for the marquis de Tillière. It spans 14 metres across the moat of the chateau. (13)

Even though concrete was discovered in Roman times and was rediscovered in the early 1800's, until the time of Monies it was not widely used not scientifically understood and accepted. Thaddeus Hyatt was the one who published a report named "An Account of Some Experiments with Portland-Cement-Concrete Combined with Iron as a Building Material, with Reference to Economy of Metal in Construction and for Security against Fire in the Making of Roofs, Floors, and Walking Surfaces", in which he reported his experiments on the behaviour of reinforced concrete. This report was to play a defining role in the evolution of concrete construction as a proven and studied science. Without Hyatt's work, more dangerous trial and error methods might been depended on for the advancement in the technology, e.g. (7) and (14).

English-born engineer Ernest Ransome was another early innovator of reinforced concrete techniques at the end of the 19th century. Using the knowledge of reinforced concrete developed during the previous 50 years, Ransome put in improvements on nearly all aspects of techniques. Ransome's key innovation was the twist of the reinforcing steel bar, thereby improving its bond with the concrete (15) . His constructions having made him widely recognized Ransome was in position to leave his mark building two of the first reinforced concrete bridges in North America (Figure 7) (16). One of the first concrete buildings constructed in the United States was a private home designed by William Ward, completed in 1876, a building designed with fire resistance in mind.

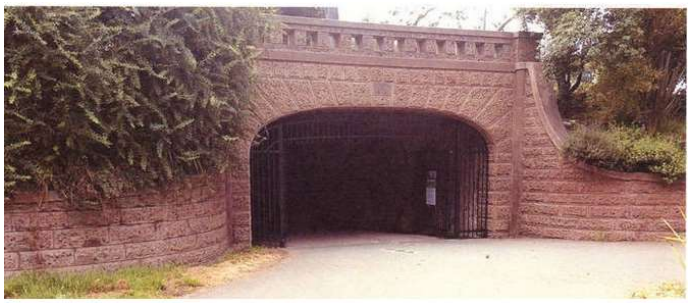

Figure 7 Constructed in 1889, the first reinforced concrete bridge in America (17)

A civil engineer from Germany bought Monier's patents and pushed forward iron and steel concrete construction. In 1884, his firm, Wayss & Freytag, made the first commercial use of reinforced concrete, e.g. (12). One of the first skyscrapers made with reinforced concrete was the 16-story Ingalls Building in Cincinnati, constructed in 1904 (10).

The first reinforced concrete building in Southern California was the Laughlin Annex in downtown Los Angeles, constructed in 1905, (18) and (19). One year later building permits were issued for reinforced concrete buildings in the City of Los Angeles, including the Temple Auditorium and 8-story Hayward Hotel, numbered 16, e.g. (20) and (21). On the same year, Bixby Hotel in Long Beach partially collapsed during construction killing 10 workers. This led to an investigation of concrete erection practices and building inspections. The structure was constructed of reinforced concrete frames with hollow clay tile ribbed flooring and hollow clay tile infill walls. That practice was strongly questioned by experts and recommendations for "pure" concrete construction were made, using reinforced concrete for the floors and walls as well as the frames (22).

Figure 8 J. Morgan's reinforced concrete structure, El Campanil, a 72-foot (22 m) bell tower at Mills College (23)

1.3 Fiber reinforced concrete

Construction materials are continuously evolving. Demand for high strength, crack, resistant and lighter concrete has resulted in the development of Fiber Reinforced Concrete (FRC). Some of the fiber materials in use are steel, nylon, asbestos, glass, carbon, sisal, jute, coir, polypropylene (24)

1.3.1 History of fiber reinforced concrete

Use of fibers for reinforcement was in use as early as the ancient world. Horse hair and straw were both utilized to strengthen the bricks (Figure 9). In 1911 use of asbestos fibers was made in concrete. In the '50s fiber reinforced concrete was becoming a field of interest as asbestos was first suspected to pose health concerns. In 1963 Romualdi and Batson publish their paper on FRC (24).

Figure 9 Horse hair in the bricks mud (25)

2.Modelling Composites: Matrix – Reinforcement

Carbon nanostructures gained the interest of researchers because of their mechanical properties. The high modulus of elasticity *E* of these materials gave to the field of mechanics promises of sky rocketing structural potential. Nanostructured composites had been successfully strengthened using carbon fibers as filling material in (26), greatly improving the mechanical properties of the matrix. Researchers have widely investigated the enhancement of graphene at both metal matrix (27) and (28), polymer matrix (29) and (30) as well as epoxy matrix nanocomposites (31).

In order to find all possible ways to use these new materials and, moreover, to optimize production methods, computational research is required; research that compares the properties of these materials for various compositions and production methods. In this way, results of the computational analysis will designate materials and combinations with properties suitable for industrial use.

The earliest attempts to calculate and predict the effective properties of heterogeneous materials were the analytical methods. Voigt made the first attempt of calculating analytically the properties (32), assuming a homogenous strain field, internally of a small unary representative sample of the material, thus making it suitable for models under axial loading. Later, Reuss followed a similar path (33), but assuming a homogenous stress field in a representative material sample, thus suitable for models under forces vertical to inclusions' axis. Eshelby created a more sophisticated model assuming infinitesimal homogenous interactions (34). This model is based on a single fiber of ellipsoid two-dimensional form inside a three-dimensional matrix of relatively large dimensions. Mori-Tanaka developed a computational theory (35) applicable to materials with inclusions of various shapes; the inclusions are considered as isolated and the strain in the matrix is considered as the out of field strain. The Mori-Tanaka method may be applied for two phase composites.

Because of increasing demand and use of composite materials with varying inclusion percentages, complex inclusion geometries and use of different kinds of inclusions

simultaneously in the same matrix, a new method of "prediction" calculation of the properties of such materials was sought. The numerical method, having no constraints in the aforementioned, was deemed suitable for modelling the microstructure of complex composite materials.

The first modelling attempts were models of a single inclusion in two-phase composites (36) not taking into consideration interactions between inclusions. Later on, the three-phase composite (37) was developed, in which the inclusion was positioned in a matrix ring which in turn was positioned in a ring of the homogenized material, the latter considered of infinite width (Figure 10). Afterwards, models were created with a small number of inclusions, according to the actual fiber packing. In such models, 9 inclusions were imported in the case where fiber packing was considered a square array, 13 inclusions in the case of a hexagonal array, and 25 fibers in such a case as of a random array, e.g. (38).

In order to succeed in simulating materials' geometrical characteristics and mechanical behaviour using RVEs, several algorithms have been developed. The most common such algorithm, the random sequential adsorption (RSA) method, was used by Babu et al. (39), implemented in MATLAB for the homogenization of carbon fibers in epoxy matrix , and by Chen et al. (40) implemented in Wolfram for homogenizing elastomer composites' properties. Savvas et al. (41) used the Monte Carlo method in order to generate a composite containing a limited number of unidirectional inclusions. The sequential addition and migration method was used by Schneider (42) to evaluate the isotropic engineering constants of glass fiber reinforced polyamide.

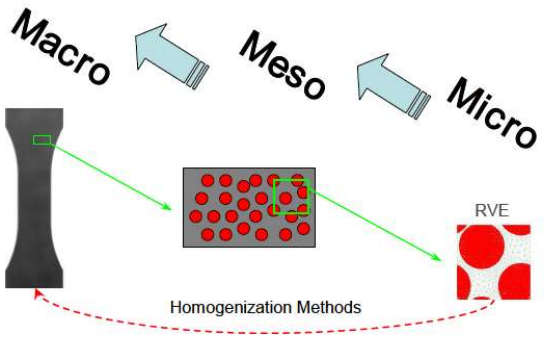

Figure 10 Homogenization Methods Overview, Ghayath Al Kassem (2009)

2.1. Semi- Analytical methods overview

2.1.1. The theoretical bounds of HILL – REUSS – VOIGT

This method is valid for a transversely isotropic symmetry (Figure 11):

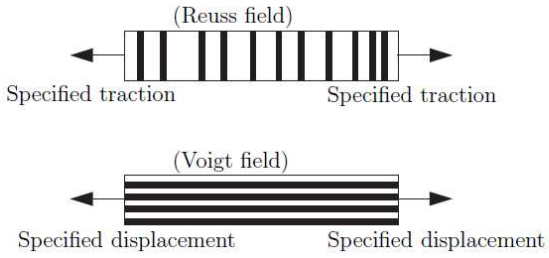

Figure 11 ***Theoretical Bounds of HILL – REUSS – VOIGT method visualization***

The Voigt's uniform strain can be calculated as follows:

$$\mathbf{C}^{Voigt} = \mathbf{C}^m + V_I\left(\mathbf{C}^I - \mathbf{C}^m\right) = V_I\mathbf{C}^I + V_m\mathbf{C}^m$$

,

while the Reuss uniform stress can be calculated as follows:

$$\mathbf{S}^{Reuss} = \mathbf{S}^m + V_I\left(\mathbf{S}^I - \mathbf{S}^m\right) = V_I\mathbf{S}^I + V_m\mathbf{S}^m$$

2.1.2. The ESHELBY Model

Eshelby solved a single-inclusion problem: An ellipsoid is cut out of an infinite matrix, undergoes an Eigen strain, and is inserted back into the matrix.

2.1.3. The MORI-TANAKA Model

The Mori-Tanaka Model proposed by Mori and Tanaka in 1973, can be applied to Isotropic and Transversal Isotropic materials (Figure 12). It takes into account interactions between the inclusions. It is accurate heterogeneous materials with a moderate volume fraction of 25-30%

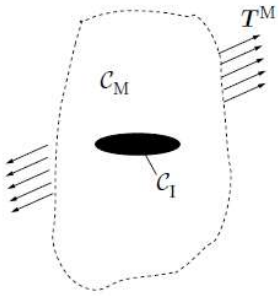

Figure 12 Mori-Tanaka Model visualization

Each inclusion behaves like an isolated inclusion, in an infinite matrix that is remotely loaded by the average matrix strain E_M or average matrix stress T_M, respectively. The concentration tensor:

$$A = [E : (C_M^{-1} C_I - I) + I]^{-1}.$$

2.1.4. The self-consistent method

This method assumes that each inclusion is isolated and embedded in a fictitious homogeneous matrix possessing the unknown macroscopic stiffness that is being searched (Figure 13).

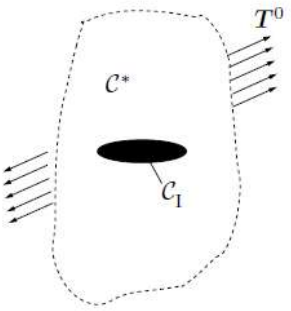

Figure 13 Self consistent method visualization

Good predictions for poly-crystals but is less satisfying in the case of two-phase composites, while the influence tensor can be calculated as follows:

$$\mathbf{A}^{SC} = \left[\mathbf{I} + \xi \mathbf{S} \left(\mathbf{C}^I - \mathbf{C}\right)\right]^{-1}$$

2.1.5. *Interpolative double inclusion model (LIELENS' model)*

This model supposes that each spheroidal inclusion (I)–of stiffness CI —is wrapped with a matrix material of stiffness CM. The outer reference material has a stiffness CR. The composite has an average or effective stiffness CLIL.

$$C^*_{(\mathrm{LIL})} = \left[\left(1 - \frac{c_\mathrm{I} + c_\mathrm{I}^2}{2}\right) C^{*-1}_{(\mathrm{MT}^{-1})} + \frac{c_\mathrm{I} + c_\mathrm{I}^2}{2} C^{*-1}_{(\mathrm{MT})}\right]^{-1}$$

From the methods that were considered during the first part of this research, the multi-step homogenization method making use of the Mori-Tanaka model was chosen. The selection was made making use of comparisons of the various analytical methods (Aboudi, 1992), Ghayath Al Kassem, 2009) and judgment of suitability of each method with regard to this specific research but also the grade by which each method is suitable to be applied in a wider range of problems.

2.2. Modelling composites using numerical method

Using the numerical method different types of elements (Figure 14) may be used for the Matrix, and Reinforcement (Fibers, sheets, platelets etc.). In present Thesis, solid 3 dimensional elements were chosen to be used for both the matrix and the reinforcement. This is the more costly –computationally- method, but one that provides the most accurate results because of the level of analysis.

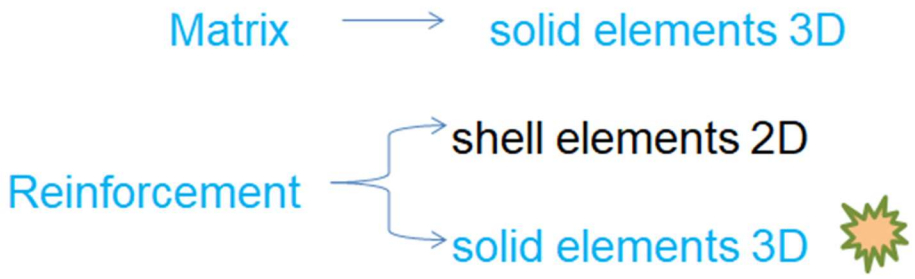

Figure 14 Numerical method element types

2.3. Cement matrix composite materials homogenization

Even though homogenization is common practice in most of the composite materials, not much research has been conducted specifically for cementitious composites. One first try to apply analytical homogenization methods in cement based concrete was made by Yang (43), who initially used the Hori and Nemat-Nasser model method to calculate the equivalent elastic moduli of the aggregate and the transition zone and then used the Mori-Tanaka model to evaluate the overall effective properties of the cement composite.

Gal and Kryvoruk (44) studied the properties of a cement based material with inclusions of both aggregates and fibers, using a two-step method. In the first step, interface transition zones and the aggregates were homogenized using an analytical model suggested by Christensen (45). In the following step, the macroscopic properties of the mortar-fibers material were evaluated using a numerical homogenization procedure.

Gal, et al (46) V-enrichment and zigzag-like enrichment functions for the shape of the inclusions or the coating and evaluated the homogenized elastic properties using 2D models of cement based materials having aggregate as inclusions surrounded by thin coatings.

Wang et al (47) applied the RVE method to cement-based composites. The algorithm that was used in order to set the fibers' orientation did not accept deleted any fiber that exceeded the boundaries and any new fiber overlapping with any of the previously placed fibers.

Zhang et al (48) used a double numerical homogenization. At the micro scale the cement matrix unit cell containing aggregate- interfacial transition zone inclusions were homogenized. At the meso-scale, the properties of the composite, consisted from fine-concrete matrix and steel fibers, were evaluated.

Qsymah et al (49) used the finite element - RVE homogenization method to define the properties of cement based composites with steel fibers of 13 mm in length and 0.2 mm in diameter and pores. Because of the dimensions of the steel fibers, that research may not be considered as at a nano-scale.

2.4. Selected homogenization methods

2.4.1 Fiber orientation

With the application of the «random orientation tensor» algorithm it becomes possible for each individual inclusion vector-among thousands that are positioned iteratively in the matrix cube- to have its own position and orientation. Each inclusion is positioned in space according to probability of convergence to the X_1, X_2, X_3 axes.

The orientation tensor, borrowed from applied fluid mechanics, provides an efficient description of fiber orientation, using a probability curve.

The tensor has nine components, with the suffixes for the tensor terms being:

- In the flow direction.
- Transverse to the flow direction.
- In the thickness direction.

Typically these axes apply:

- The X-Y (or 1-2) flow plane.
- The Z-axis in the thickness direction, out of the 1-2 flow plane.

In order to achieve a higher randomization of the placement of inclusions in the three-dimensional cube, the following values were used for the orientation tensor α_{11}= 0.333, α_{22}= 0.333, α_{33}= 0.333 with all other components left as null. In Figure 15 the created micro structure geometry - as seen in the ANSA software environment - for the case of the aforementioned tensor values is displayed.

a) $$a_{ij} = \begin{bmatrix} a_{11} & a_{12} & a_{13} \\ a_{21} & a_{22} & a_{23} \\ a_{31} & a_{32} & a_{33} \end{bmatrix}$$

b) 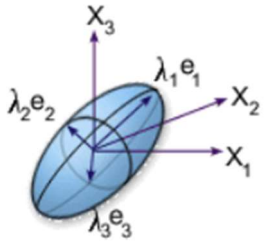

c) 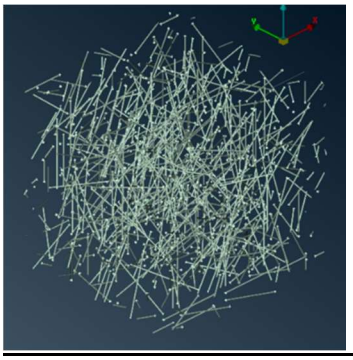

d) 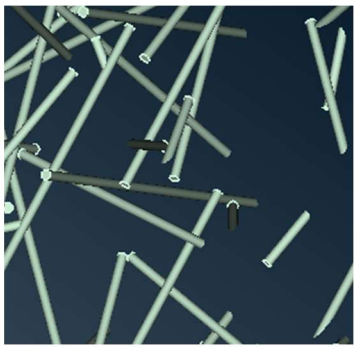

Figure 15 Orientation tensor a) tensor b) geometric representation c,d) orientation representation (not actual inclusion sizes)

The flow direction orientation term, contains most of the quantitative information about the microstructure and is most sensitive to flow, processing and material changes (ANSYS documentation). In the pictures of Figure 15c, Figure 15d, Figure 16 are shown examples of ANSA model representation for random orientation tensor. Radius of fibers is exaggerated for the purposes of better presentation.

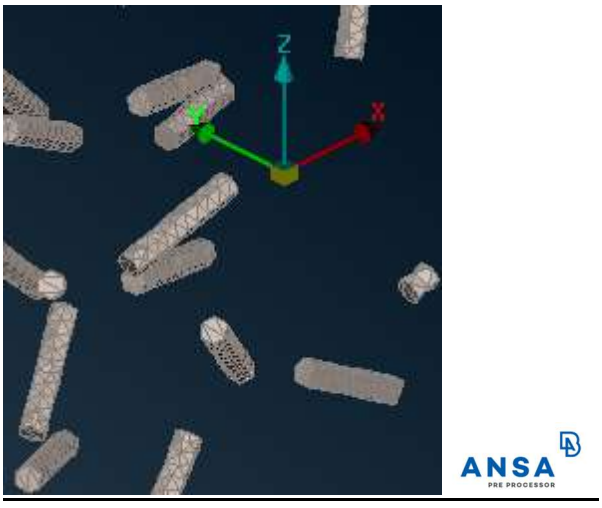

Figure 16 Orientation Tensor model representation

Another way to simulate fiber orientation is by using Fixed Phi Theta Angles (Figure 17).

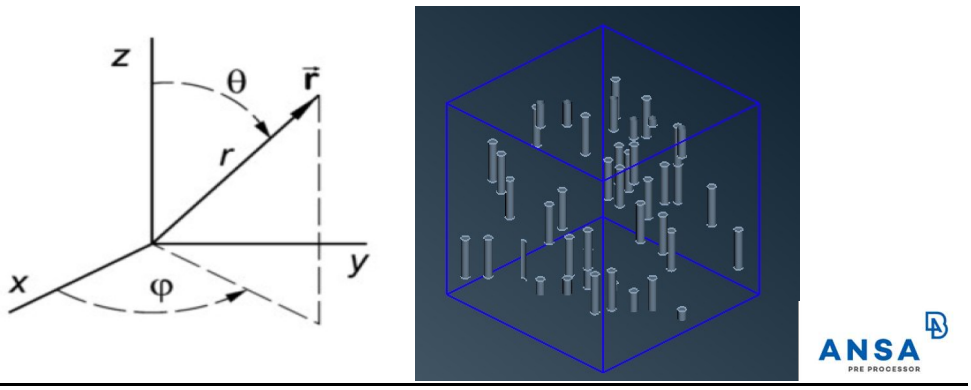

Figure 17 Fixed Angle Fiber Orientation, left: geometry, right: ANSA representation

Fixed Phi Theta Angle combinations used in this research:

- Φ= 0 , θ= 0
- Φ= 0 , θ= 45
- Φ= 0 , θ= 90
- Φ= 0 , θ= -45
- Φ= 45 , θ= 0
- Φ= 45 , θ= 45
- Φ= 45 , θ= 90
- Φ= 45 , θ= -45
- Φ= 90 , θ= 0
- Φ= 90 , θ= 45
- Φ= 90 , θ= 90
- Φ= 90 , θ= -45
- Φ=-45 , θ= 0

- Φ=-45 , θ= 45
- Φ= 45 , θ= 90
- Φ=-45 , θ= -45

The above 16 phi theta angle combinations were used for the inclusions, each for equal volume fractions, representing a kind of “ideal” dispersion, as seen in Figure 18.

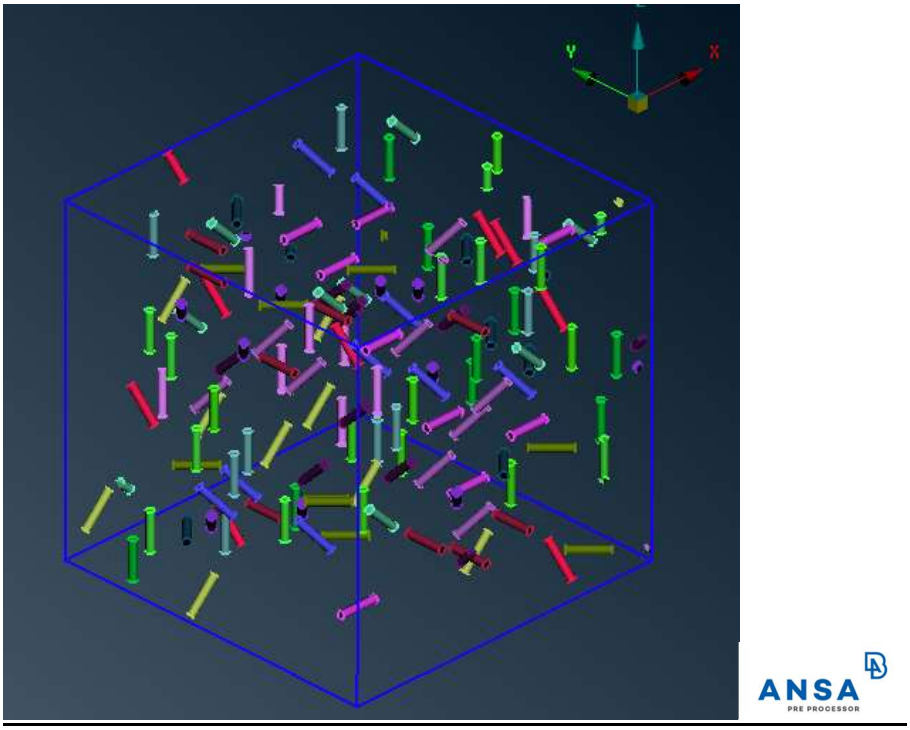

Figure 18 Fixed Angle Fiber Orientation result presented with ANSA

2.4.2 Periodic geometry algorithm

For the purposes of this research the so called “periodic geometry algorithm” was used. Periodicity across surfaces means that continuity between adjustment RVEs is ensured. The way this is achieved by, is that inclusions in the RVE that intersect the cube outer surfaces, are “cut” with the remainder being placed as continuing from the opposite surface. Additionally, the algorithm takes into account a minimum separation distance between the surfaces of any two inclusions. This ensures that desired volume fraction is more effectively achieved and fibers dispersion is more realistic.

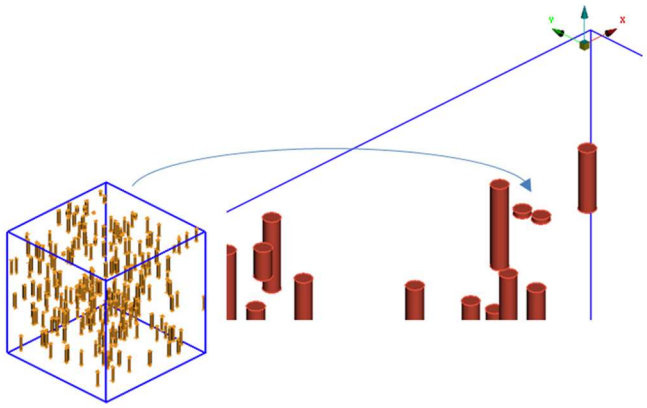

Figure 19 Periodic Geometry Algorithm result representation

2.4.3 Nano-scale Homogenization model

Two procedures may be followed, one for the isotropic case with two independent parameters (E, v) and one for the transverse isotropic case with five independent parameters (E_{11}, v_{12}, E_{22}, v_{23}, G_{12}). For the isotropic case:

i) tensile perturbation in the x-direction gives

$$E^{eff} = E_{11}^{eff} = \frac{\langle \sigma_{11} \rangle_{\Omega_0}}{\langle \varepsilon_{11} \rangle_{\Omega_0}}$$

$$v_{12}^{eff} = -\frac{\langle \varepsilon_{22} \rangle_{\Omega_0}}{\langle \varepsilon_{11} \rangle_{\Omega_0}}; v_{13}^{eff} = -\frac{\langle \varepsilon_{33} \rangle_{\Omega_0}}{\langle \varepsilon_{11} \rangle_{\Omega_0}}$$
$$v^{eff} = \left(v_{12}^{eff} + v_{13}^{eff}\right)/2$$

ii) tensile perturbation in the y-direction gives

$$E^{eff} = E_{22}^{eff} = \frac{\langle \sigma_{22} \rangle_{\Omega_0}}{\langle \varepsilon_{22} \rangle_{\Omega_0}}$$

$$v_{21}^{eff} = -\frac{\langle \varepsilon_{11} \rangle_{\Omega_0}}{\langle \varepsilon_{22} \rangle_{\Omega_0}}; v_{23}^{eff} = -\frac{\langle \varepsilon_{33} \rangle_{\Omega_0}}{\langle \varepsilon_{22} \rangle_{\Omega_0}}$$
$$v^{eff} = \left(v_{21}^{eff} + v_{23}^{eff}\right)/2$$

and

iii) tensile perturbation in the z-direction gives

$$E^{eff} = E_{33}^{eff} = \frac{\langle \sigma_{33} \rangle_{\Omega_0}}{\langle \varepsilon_{33} \rangle_{\Omega_0}}$$

$$\nu_{31}^{eff} = -\frac{\langle \varepsilon_{11} \rangle_{\Omega_0}}{\langle \varepsilon_{33} \rangle_{\Omega_0}}; \nu_{32}^{eff} = -\frac{\langle \varepsilon_{22} \rangle_{\Omega_0}}{\langle \varepsilon_{33} \rangle_{\Omega_0}}$$

$$\nu^{eff} = \left(\nu_{31}^{eff} + \nu_{32}^{eff}\right)/2$$

The RVE was subjected to three tensile and three shear loadings using the Epilysis solver software. The ANSA Homogenization Tool ensures distribution of hundreds of inclusions in the RVE according to the volume fractions of the experimental data used as basis. The Homogenization tool also ensures that an appropriate number of finite elements are placed adjusted to each inclusion's sides in order to keep the RVE's loading results unaffected from element size, and as a result, the calculated properties of the homogenized material. The option of an even thicker than suggested by the Homogenization Tool mesh is open and it was indeed taken for the purposes of this research, Cross – checking for different random orientation positioning results was conducted, and for every different geometric position of the inclusions the results remained constant.

The Multi-Step Homogenization Method

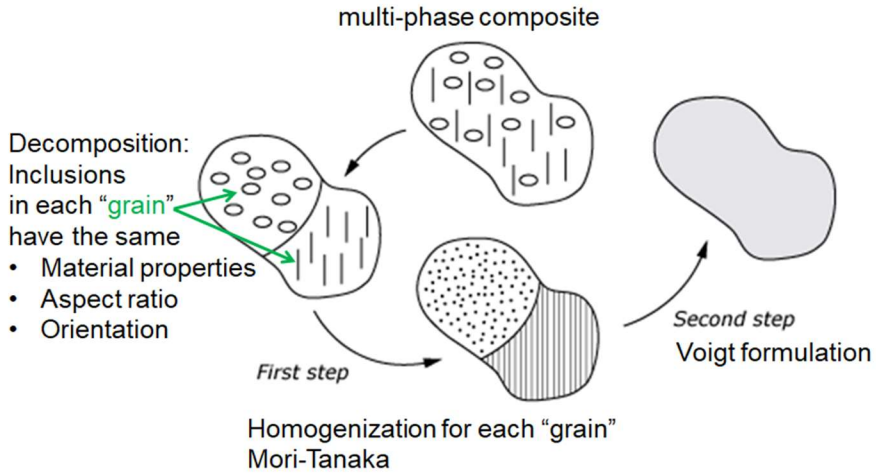

Figure 20 Multi Step Homogenization Method representation, Abaqus documentation

Adhering to the multi-step homogenization method, the composite is decomposed into "grains", with each grain containing one inclusion family and the matrix. The inclusions in each family have the same material properties, aspect ratio, and orientation. In the first step homogenization is performed in each grain using the Mori Tanaka model; in the second step the Voigt formulation is used to compute the properties of the overall composite.

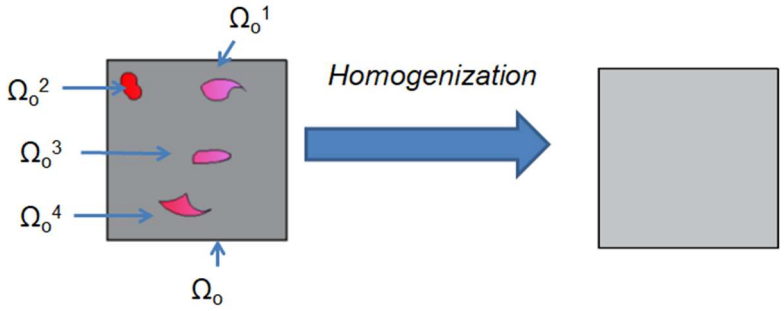

Figure 21 Representative Volume Element homogenization method representation

The representative volume element (RVE) is a sample of the material microstructure that the macroscopic body consists of as shown in. In order to be representative, the size of the RVE is of great importance. A definite perturbation is applied to calculate a definite material property. Two procedures may be followed, one for the isotropic case with two independent parameters (E, v) and one for the transverse isotropic case with five independent parameters (E_{11}, v_{12}, E_{22}, n_{23}, G_{12}).

3. Research methodology

3.1 Experimetal data

As a basis for this paper experimental data were gathered from the experimental results drawn from the research investigation of Prof. Z. S. Metaxa, e.g. (50), (51) and (52). These papers describe the experiments of specimens subjected to three point bending flexural tests. The specimens were of a cement paste matrix with multi walled carbon nanotube (MWCNT) inclusions of various volume percentages, between 6 and 20 per mille. Preparation of cement paste was documented. The MWCNTs were either all of a short or of a long type shape. The preloaded specimens were notched in the middle (Figure 22). Further characteristic values and data are shown in the figures and table below.

The modulus of elasticity of the cement matrix used in those experiments was calculated as having a value of 4000 MPa. In the same experiments both long and short fibers were used as inclusions, with characteristics as shown in Table 1. Even though the methodology was applied to both types of inclusions, this paper focuses in the use of short fibers. Data was available for inclusion volume fractions of 6 and 12 ‰.

Table 1 General characteristics of Multi Walled Carbon Nanotubes used in experiments

	Aspect Ratio	Diameter (nm)	Length (μm)	Purity (%)	Specific surface area (m2/g)
Short (Cheap Tubes®)	700	20-40	10-30	>95	110
Long (Nanothings®)	1600	20-40	10-100	>97	250-300

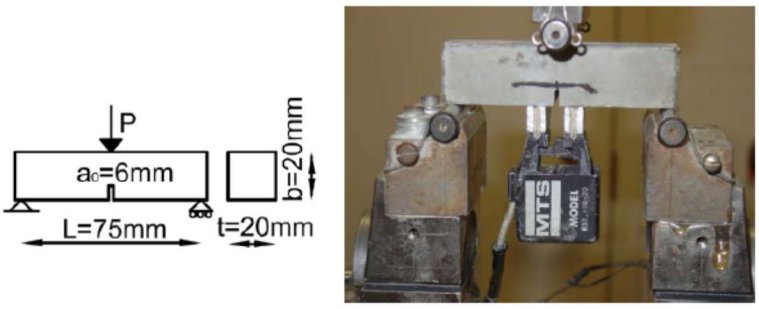

Figure 22 left: Diagramme of the three-point flex notched specimen and right: picture of the three-point bending flexural test fixture

In all experiments the crack mouth opening displacement was measured. Results were plotted into graphs such as that of the example below (Figure 23).

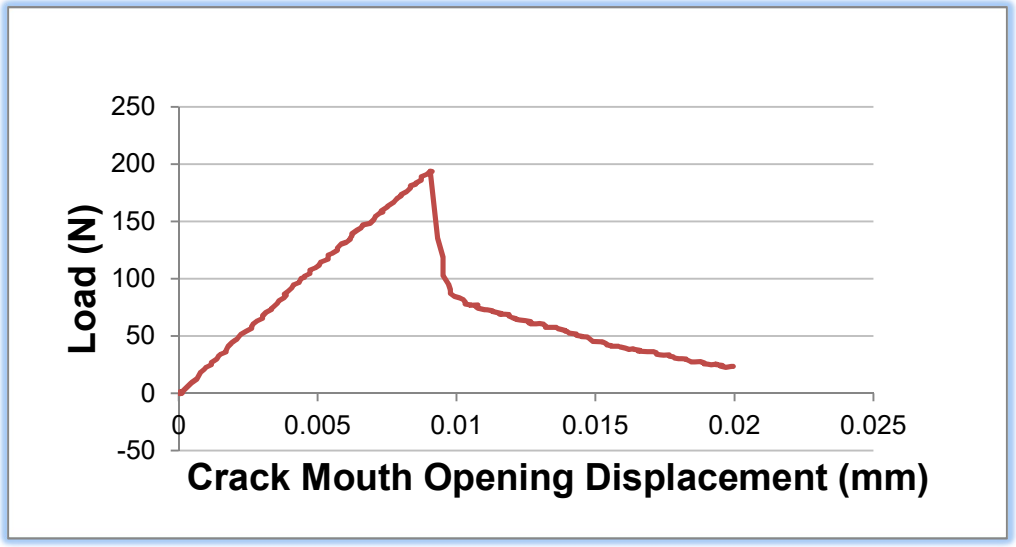

Figure 23 Plot of experimental results for the short fibers – 6‰ combination

Representative values for the modulus of elasticity of the carbon nanotubes were taken from Min-Feng Yu, et al (2000) (53), a research of the same era as the experiments, ensuring similar production techniques. These values are shown in **Σφάλμα! Το αρχείο προέλευσης της αναφοράς δεν βρέθηκε.**.

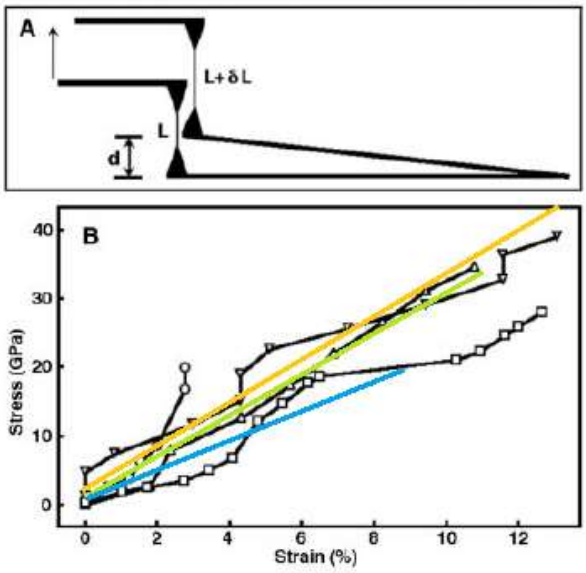

CNT Modulus of Elasticity:

- E=274 GPa
- E=335 GPa
- E=470 GPa

Figure 24 Representative values for modulus of elasticity of inclusions (53)

3.2 Research methodology

For the numerical method, a Representative Volume Element was used in order to achieve homogenization. The RVE was subjected to three tensile and three shear loadings using the Epilysis solver software (Figure 25).

a. 3 tensile loadings

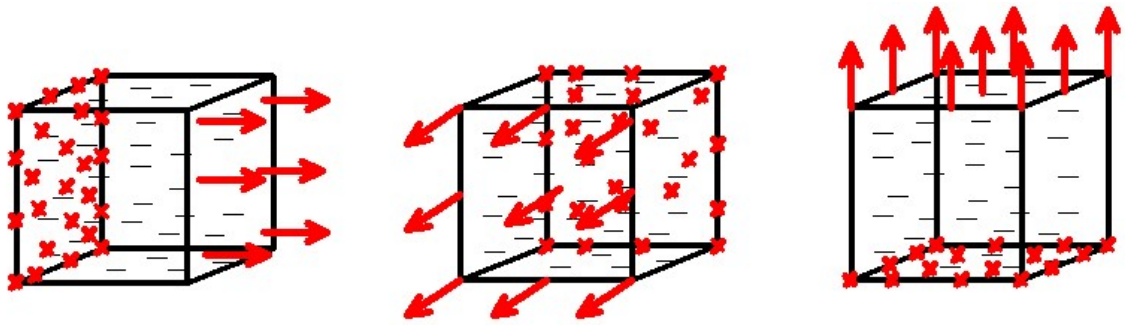

b. 3 shear loadings

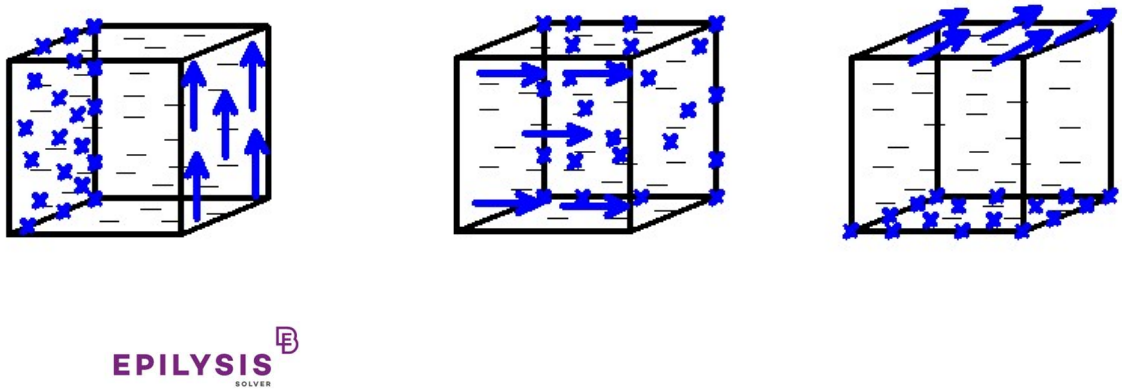

Figure 25 RVE loading procedure a. tensile b. shear

From these 6 loadings, strain – stress results were obtained. Those were in turn used to calculate the effective modulus of elasticity of the composite. Following (Figure 26) is a representation of the existing crack mouth as modeled.

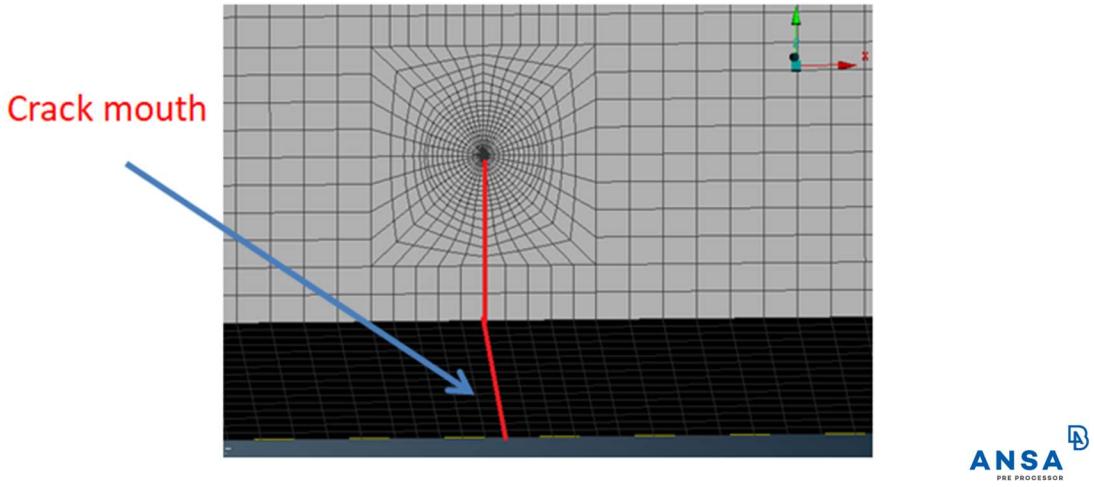

Figure 26 Pre-existing crack mouth opening representation

The lips were modeled in contact with each other in the beginning of the experiment. After loading, the crack mouth opening displacement would be of the form shown in the example below (Figure 27b):

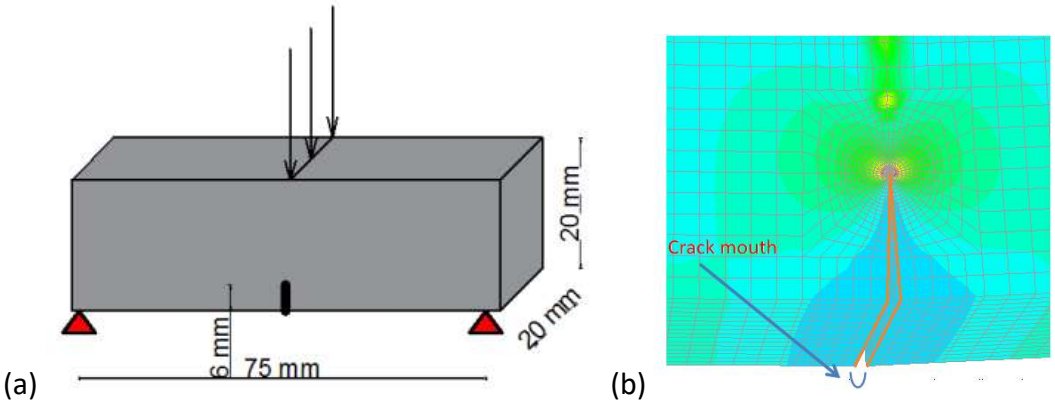

Figure 27 (a) Model geometry and b) FE discretization near the crack tip.

The following procedure was followed in order to obtain the properties of the unreinforced matrix corresponding to those of the experiment. The unreinforced cement matrix was modeled using finite elements (Figure 28).

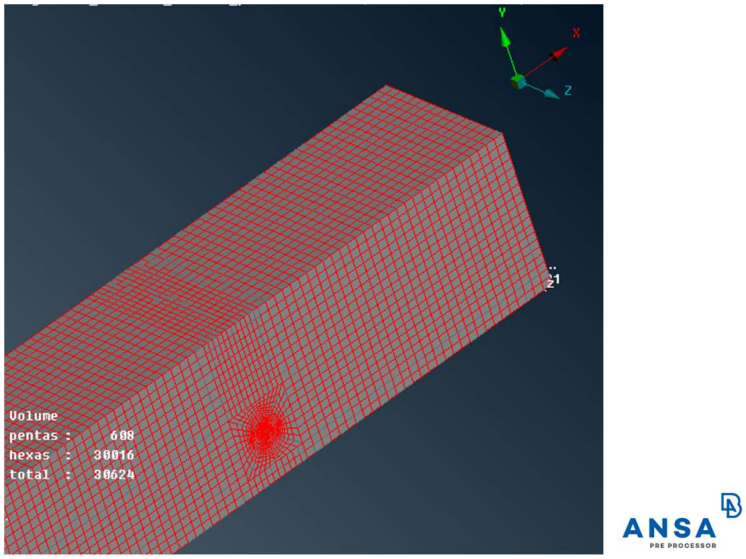

Figure 28 Unreinforced cement matrix model

Then the experiment was simulated with the same conditions as shown in Figure 29.

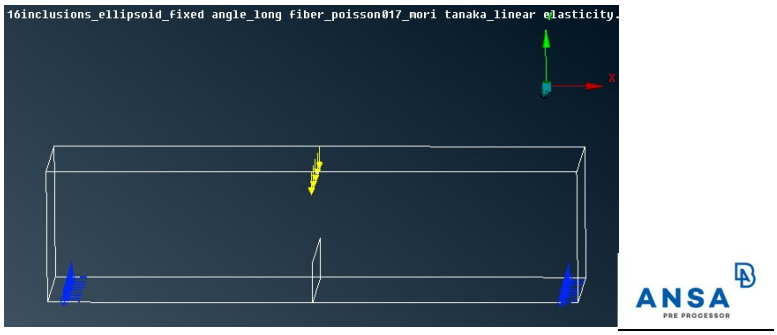

Figure 29 Specimen geometry, loading and boundaries

Then various values were given to the modulus of elasticity, until the unreinforced matrix's behaviour became nearly identical to that described by the experimental results.

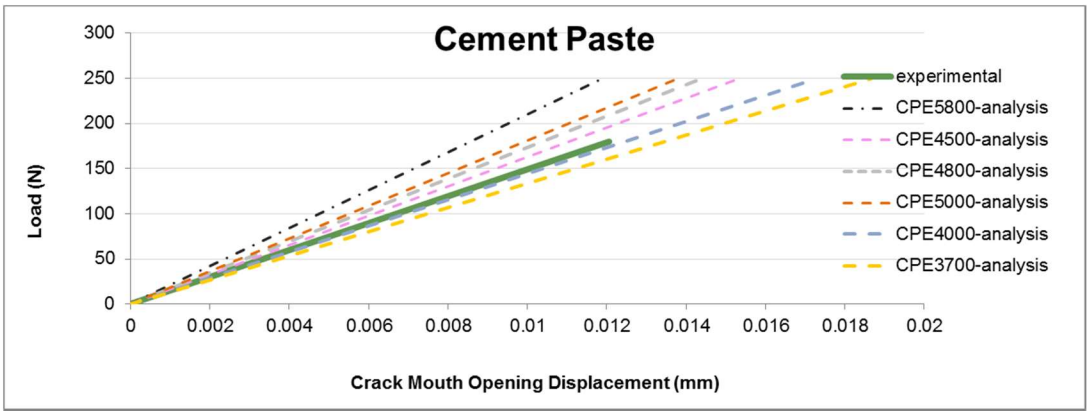

Figure 30 CMOD – load simulation results

As seen in the plot above (Figure 30), such behaviour was obtained for a modulus of elasticity of 4000 MPa. The methodology flowchart is shown in Figure 31. For – available from experiments – inclusion volume fractions (V_f) of 0.6 and 1.2 % the following steps were followed:

i. Selection of CNT Poisson ratio (starting value is the highest found in literature, i.e. 0.35)

ii. Selection of CNT modulus of elasticity (E_{CNT}) (starting value is the lowest found in literature, i.e. 235 GPa according the results in (53).

iii. Calculation of the Homogenized Material Stiffness Matrix: RVE finite element along with the random orientation tensor, as described in the previous chapter of homogenization methodology.

iv. Modeling of the pre-cracked specimens using the aforementioned Homogenized Matrix and Simulation of the experiment (FE).

v. Measurement of the Crack Mouth Opening Displacement in the CAE models.

vi. Comparison of the Crack opening displacement with experimental results.

vii. Change to higher CNT modulus of elasticity.

viii. New loop from step 2 until satisfactory deviation from experimental results (or until reaching non-realistic values of E_{CNT}, with the latter not having been applicable in this paper).

ix. Change to lower CNT Poisson ratio.

x. New loop from step 1 until satisfactory deviation from experimental results (or until reaching non-realistic values of v_{CNT}).

xi. Determination of Poisson's ratio and modulus of elasticity values from results closest to experimental for experimental inclusion volume fractions.

xii. Expressing the composite material's $E_{effective}$ as a function of the inclusion volume fraction (V_f).

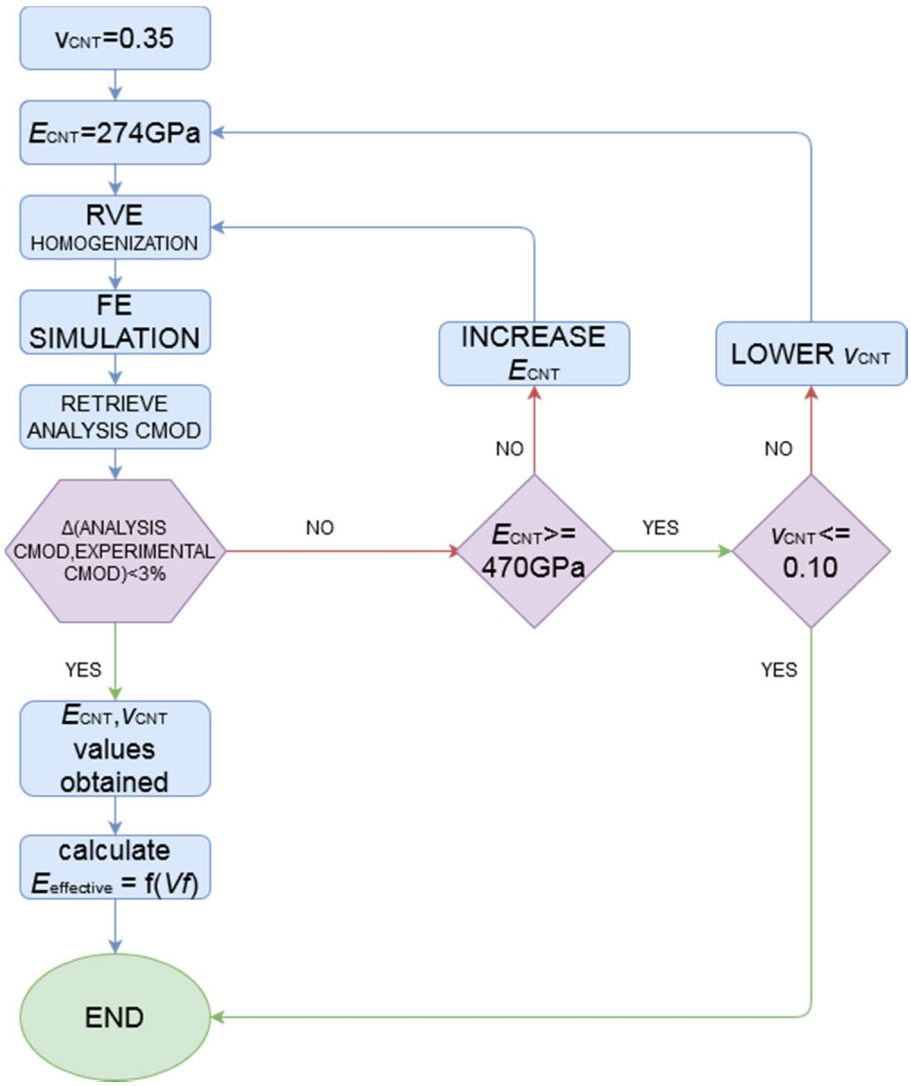

Figure 31 The flowchart of the methodology used in the present investigation.

4. Results

In the present Thesis, the 'appropriate' combination of homogenization methods and fiber orientation resulted in the more accurate predictions of the mechanical behaviour expected from the experimental results is investigated. As can be seen in the following figures, Figure 32, Figure 33, Figure 34**Σφάλμα! Το αρχείο προέλευσης της αναφοράς δεν βρέθηκε.** and Figure 35, the random orientation tensor was better in providing that accuracy and in comparison between the combinations of finite element method – random orientation tensor and multi-step homogenization – random orientation tensor, the "pure" finite element method proved to provide the outmost accuracy from all other combinations.

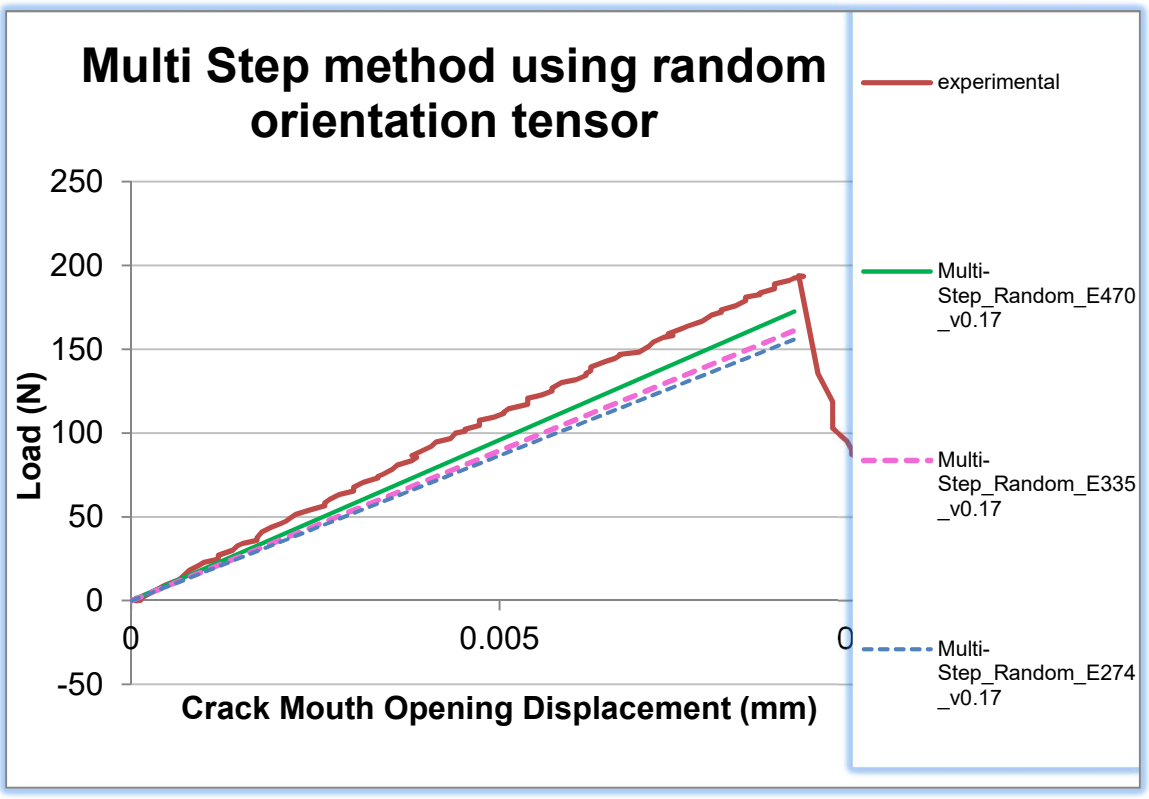

Figure 32 Multi step method using random orientation tensor

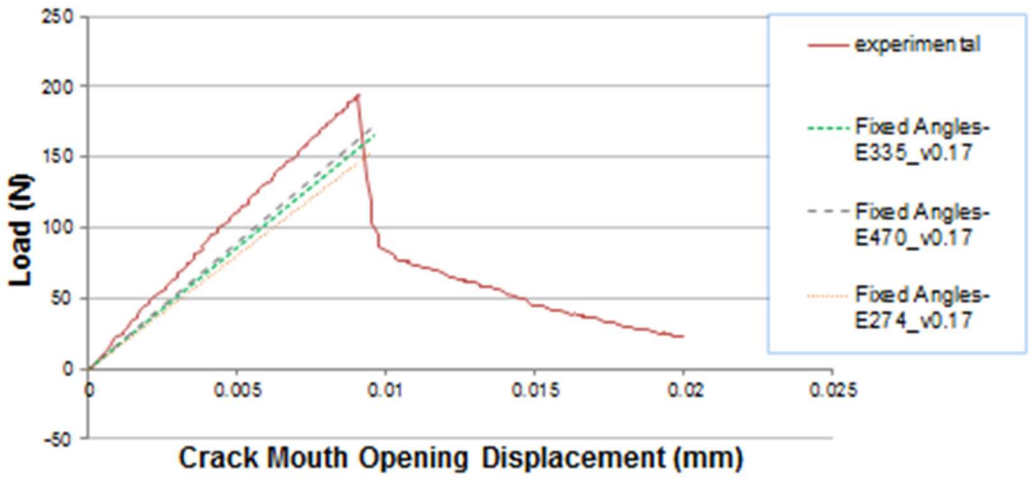

Figure 33 Finite element method using fixed angles

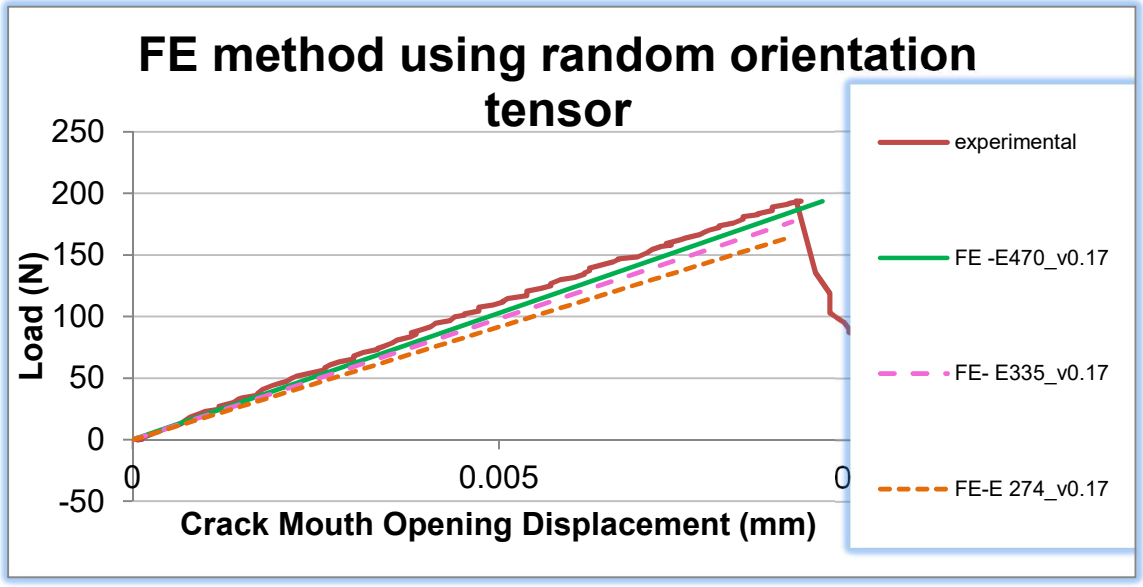

Figure 34 Finite element method using random orientation tensor

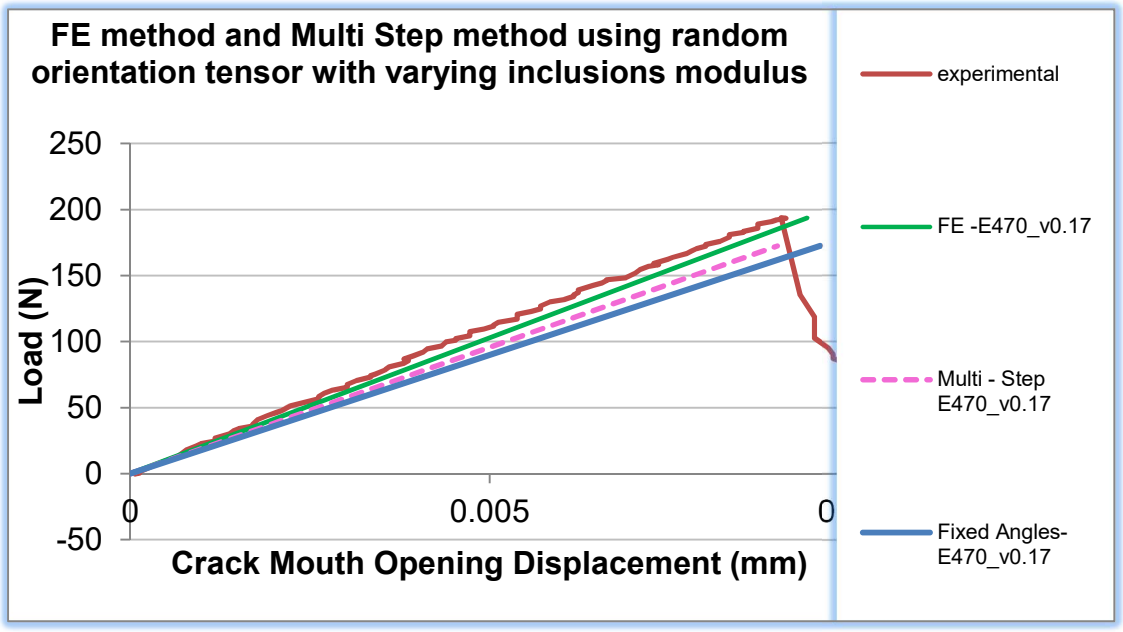

Figure 35 Finite element method and multi-step method using random orientation method

4.1 Effect of CNTs' Poisson's ratio

Regarding steps (i) and (x) of the methodology followed, as was already stated modelling started with v_{CNT} value of 0.45. As the value of Poisson's ratio was lowered –all other parameters constant, the resulting simulation of showed a CMOD value closer to that of the experimental results. For example (Figure 36), for a V_f = 0.006 and E_{CNT}=470 GPa the following progress was observed: in order for a CMOD value of 0.009058 mm to be observed, Loading for the experiments was at 193.8296 N. For the same CMOD value to be observed in a simulation with v_{CNT} = 0.35, loading of 177.771 N was required- a deviation of 0.082849 from experimental value; with v_{CNT} =0.17, loading of 186.2442 N, deviation of 0.039135 from experimental results, an improvement of 4.3715 %; with v_{CNT} = 0.10, loading of 189.7917 N, deviation of 0.020832 from experimental results, an improvement of 1.8302 %. At this point both the improvement rate reached values too small and v_{CNT} values were very low compared to experimental results in literature to allow for further simulations with lower v_{CNT} values.

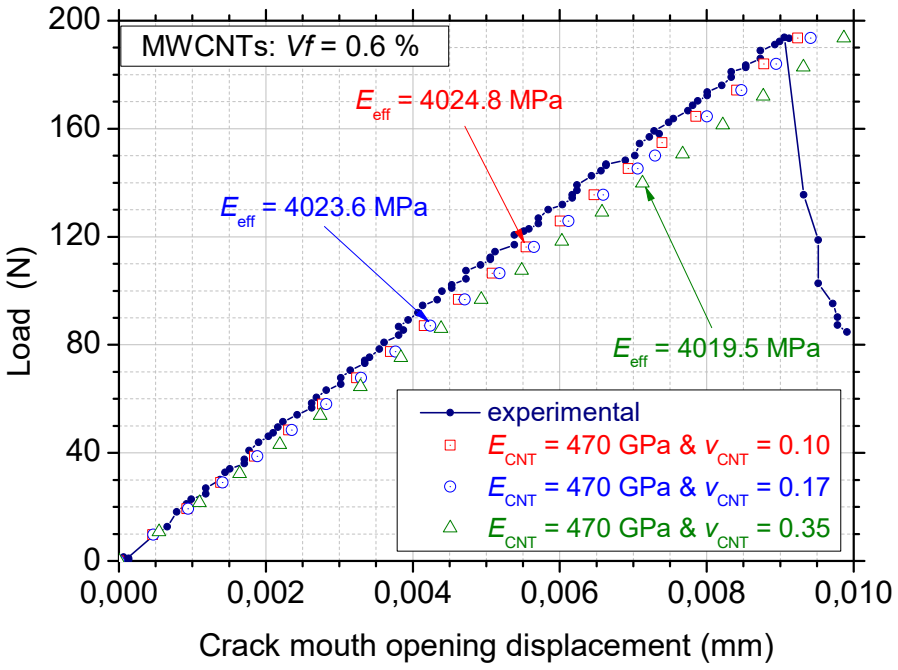

Figure 36 Diagram of applied load against CMOD for the same cement-based material matrix reinforced with V_f = 6 ‰ MWCNTs, E_{CNT} = 470 GPa and comparing Poisson ratio of the CNTs (ν_{CNT} = 0.10, 0.17, 0.35).

Figure 37 shows the same process for identical parameters, except for the inclusion volume fraction which now receives the other available from experimental data value of V_f = 12 ‰.

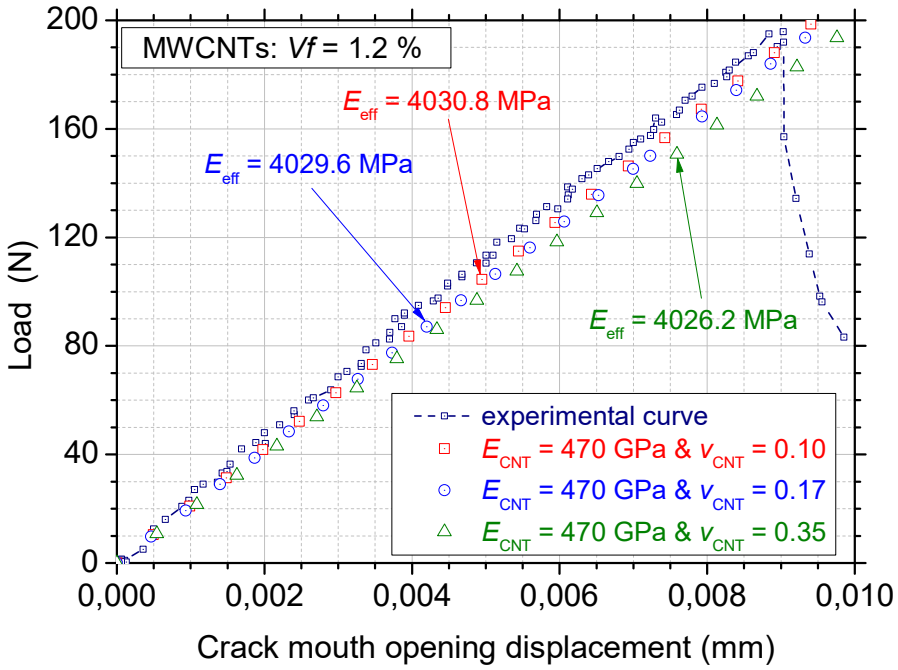

Figure 37 Diagram of applied load against CMOD for the same cement-based material matrix reinforced with V_f = 12 ‰ MWCNTs, E_{CNT} = 470 GPa and comparing Poisson ratio of the CNTs (ν_{CNT} = 0.10, 0.17, 0.35).

4.2 Effect of CNTs' modulus of elasticity

Similar to the previous steps, the E_{CNT} steps started for a value of 274 GPa and stopped at 470 GPa; the values of GPa being close to the experimental ones, and further simulations with higher E_{CNT} values giving minimal rate of convergence to the experimental data. The optimal loop was the combination of v_{CNT}=0.17 and E_{CNT} = 470 GPa, as seen in the figures for a V_f of 6 ‰. The optimal loop parameters remained the same for the other experimental V_f value of 12 ‰.

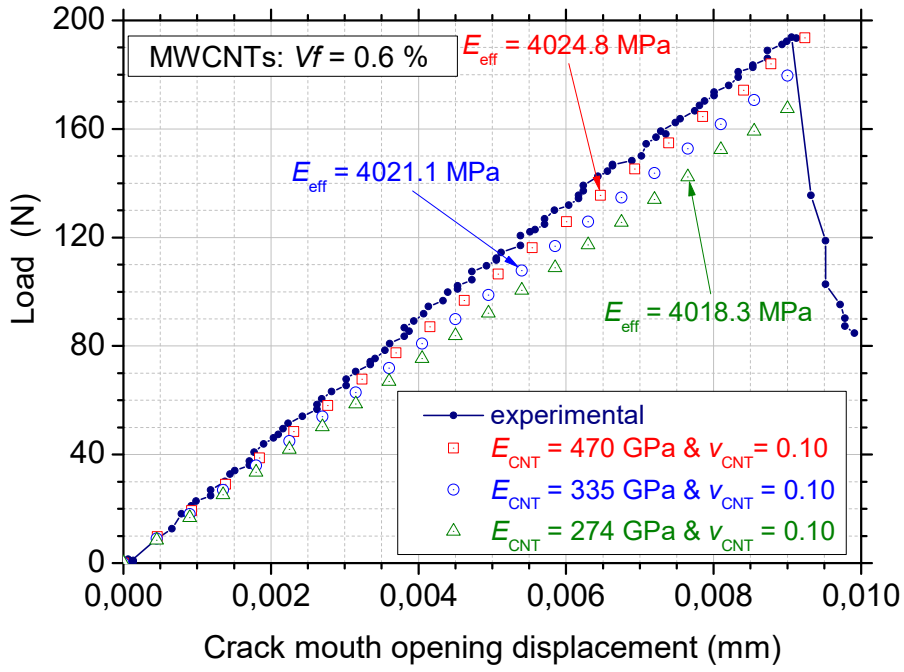

Figure 38 Diagram of applied load against CMOD for the same cement-based material matrix reinforced with V_f = 6 ‰ MWCNTs, Poisson ratio of the CNTs (v_{CNT} = 0.10) and comparing modulus of elasticity of the CNTs (E_{CNT} = 274, 335 and 470 GPa).

In Figure 38 and Figure 39, a comparison of the effective moduli of elasticity calculated from the simulations can be seen for various parameter combinations. As discussed the optimal combination for both available experimental inclusion volume fractions was that of E_{CNT} = 470 GPa / v_{CNT} = 0.17; optimal meaning that being as close as possible to the experimental data with any further calibrations giving minimal gains.

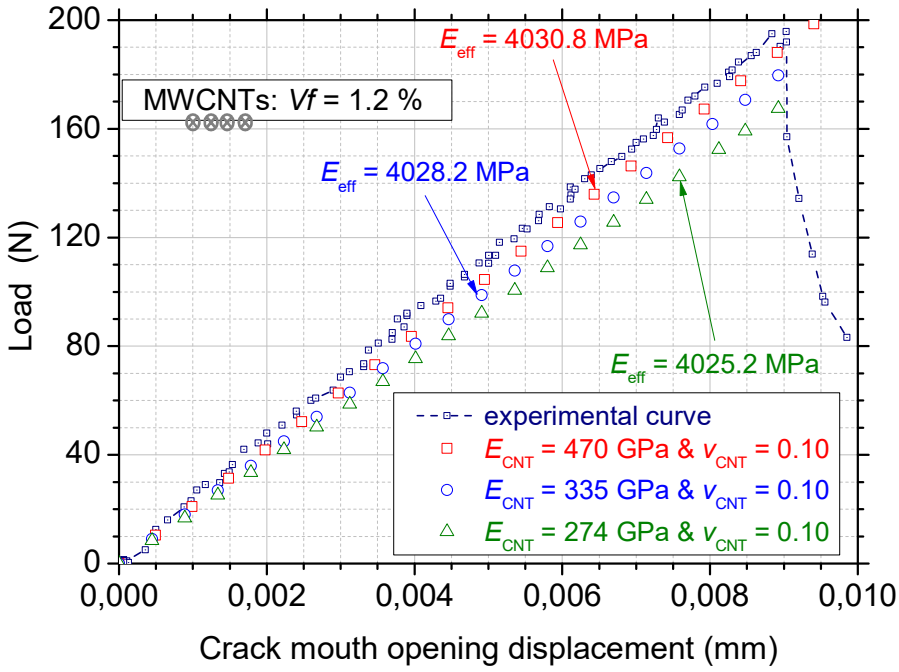

Figure 39 Diagram of applied load against CMOD for the same cement-based material matrix reinforced with V_f = 12 ‰ MWCNTs, Poisson ratio of the CNTs (ν_{CNT} = 0.10) and comparing modulus of elasticity of the CNTs (E_{CNT} = 274, 335 and 470 GPa).

Selecting from each homogenization method the combination that comes closer to the experimental results and plotting them in Figure 40.

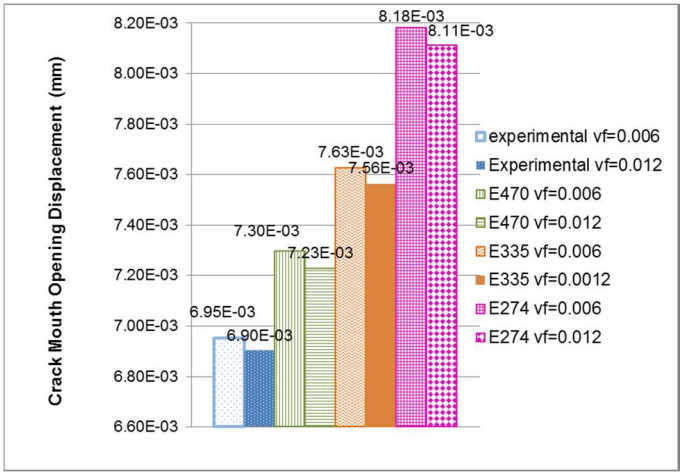

Figure 40 Column chart comparing simulation and experimental CMODs under the same loading of 150 N for various E_{CNT} and V_f values

5. Optimization of the graphene reinforcement in cement-based materials

In a case where a researcher or an engineer is considering the use of various combinations of inclusion materials and/or inclusion geometries and/or inclusion volume fractions and or matrix materials, this methodology may be applied in reverse, constraining the design properties the composite material must exhibit in order to be suitable for the application. Where density is a factor, it may be used for exclusion of those combinations that do not meet the constraints.

The Interior Point Optimization (IPOpt) algorithm is used for the iterations applied to the effective modulus of elasticity of the homogenized material. The effective modulus of elasticity is assumed as volume fraction dependent and is calculated at every iteration using the multi-Step method, with the ANSA® homogenization tool. Where *x* variable is the CNT volume fraction (Eq 2), objective *f*(x) is the difference between the E_{eff} calculated by the homogenization within the current iteration and the target E_{eff} (Eq. 3), g_L and g_U are the lower and upper constraints bounds (Eq. 4), and x_L and x_U are the lower and upper variable bounds (Eq. 5). At every cycle, a new volume fraction is set, and a new objective is recalculated. The points x which satisfies the constraints (inequality) lower and upper bounds (g_L and g_U in Eq. 4) are considered as feasible. At every cycle the new volume fraction value must range between the x_L and x_U bounds (Eq. 5). Convergence is achieved when either the objective value is less than a limit objective value or the maximum number of iterations has been completed.

$$x \in \mathbb{R}^n, \qquad x = vf_{CNT} \tag{2}$$

$$\min f(x), \qquad f(x) = E_{eff}^{calculated} - E_{eff}^{target} \tag{3}$$

$$g\_L < g(x) < g\_U \tag{4}$$

$$x\_L < x < x\_U \tag{5}$$

The steps to be followed for the optimal volume fraction identification using the proposed method, as shown in Figure 41, are:

i. Set target effective modulus ($E_{\text{eff}}^{\text{target}}$) of the Homogenized Material, set boundaries for volume fraction.

ii. Set initial point for the IPOpt. The initial point is the initial value of the CNT volume fraction.

iii. Calculate effective modulus ($E_{\text{eff}}^{\text{calculated}}$) of the Homogenized Material (given E_{CNT}, v_{CNT}, E_{cement}, v_{cement}, initial volume fraction) using multi-Step method combined with Representative Volume Element (RVE) method at ANSA® Pre-Processor.

iv. Evaluate the difference between the calculated effective modulus and the target effective modulus ($E_{\text{eff}}^{\text{calculated}} - E_{\text{eff}}^{\text{target}}$) of the Homogenized Material

v. If the difference is more than limit objective value and the number of the completed iterations is less than the maximum number of iterations move on to the next iteration.

vi. Set new volume fraction value.

vii. Start the new iteration using the next point for the IPOpt.

viii. Calculate of the Homogenized Material ($E_{\text{eff}}^{\text{calculated}}$) of the Homogenized Material (given E_{CNT}, v_{CNT}, *E*cement, *v*cement, new volume fraction) using multi-Step method combined with RVE at ANSA® Pre-Processor

ix. If the difference $E_{\text{eff}}^{\text{calculated}} - E_{\text{eff}}^{\text{target}}$ is less than limit objective value or the number of the completed iterations are or than the maximum number of iterations move on to the next iteration.

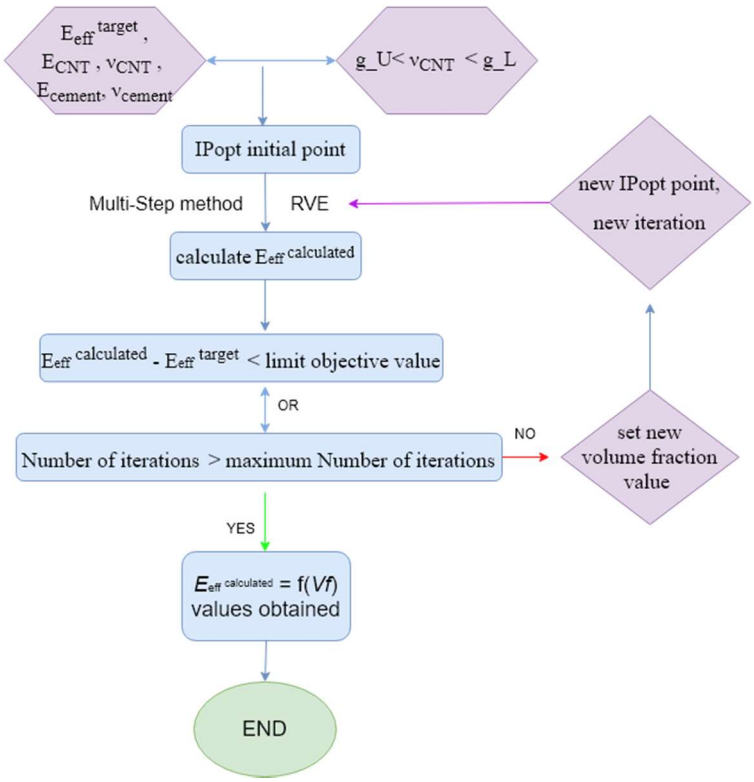

Figure 41 Optimization Methodology flowchart

The aforementioned steps were followed for three optimization cases of iterations and different objective value. In the first case, the maximum number of iterations was 20 and the maximum objective value 5 MPa. In the second case, the maximum number of iterations was 200 and the maximum objective value 1 MPa (Figure 42). In the third case, the maximum number of iterations was 1000 and the maximum objective value 1e-4 MPa (Figure 43).

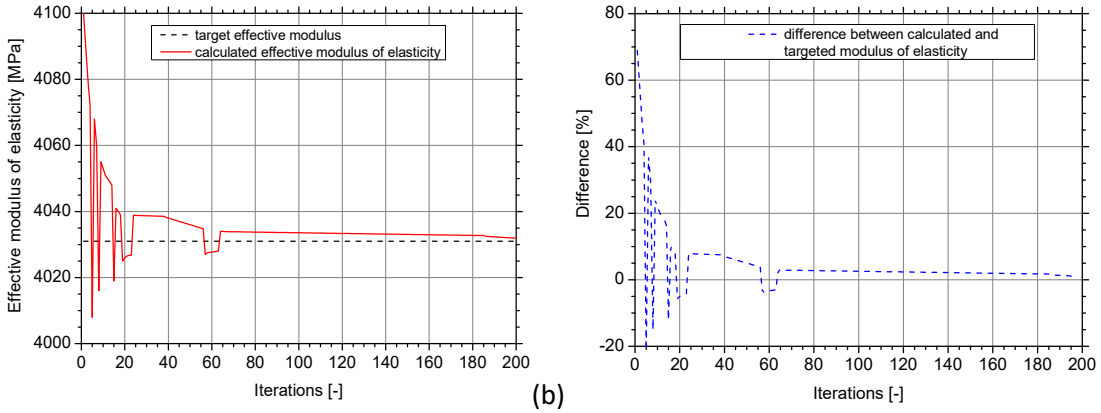

Figure 42 (a) Effective modulus of the optimization for 200 maximum iterations and maximum objective value 1 MPa; (b) difference between calculated and target effective modulus of the optimization case for 200 maximum iterations and maximum objective value 1 MPa.

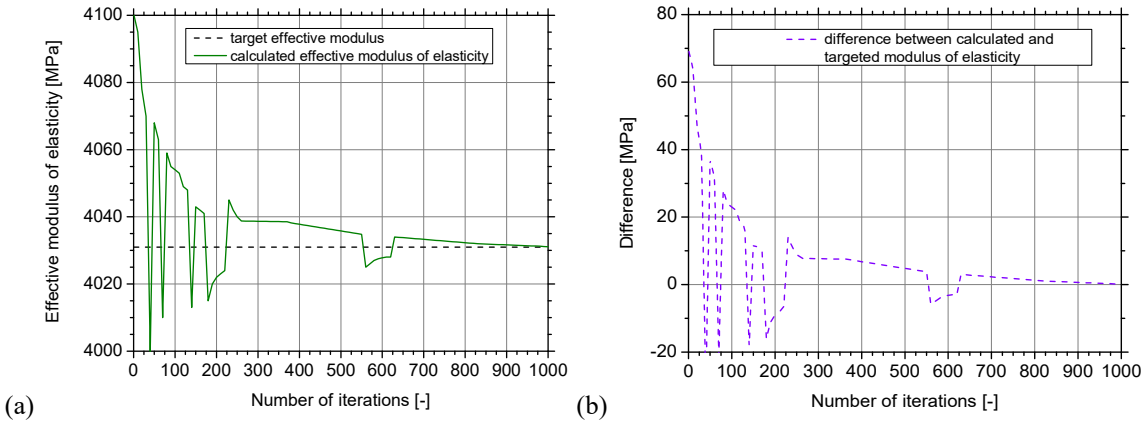

Figure 43 (a) Effective modulus of the optimization case for 1000 maximum iterations and maximum objective value 1e-4 MPa; (b) difference between calculated and target effective modulus of the optimization case for 1000 maximum iterations and maximum objective value 1e-4 MPa.

6. Conclusions

6.1 Homogenization method

From the simulation results, the following equation describing the E of any composite material with the same matrix and inclusion type E ($E_{effective}$) as a function of the inclusion volume fraction (V_f).

$$E_{effective} = 2E\text{-}06\ \boldsymbol{V_f}^6 - 0.0005\ \boldsymbol{V_f}^5 + 0.0384\ \boldsymbol{V_f}^4 - 1.4715\ \boldsymbol{V_f}^3 + 26.441\ \boldsymbol{V_f}^2 + 915.74\ \boldsymbol{V_f} + 4019$$

Equation 1 Estimation of effective modulus E of the homogenized material with respect to V_f of CNTs

The equation of $E_{effective}$ (Equation 1) describes any such composite with the same materials but different inclusion volume fraction. The optimal point where each loop described in the methodology should stop may change according to accuracy required and/or available computational power and time.

The same methodology may be used to model any composite of certain parameters, with known matrix properties, regardless of inclusion shape/geometry and properties even with combinations of different inclusion types.

The loops in the methodology allow for calculation of the composite properties even with unknown inclusion properties, meaning that as long as experimental data are available, the methodology can still be applied and during the steps permits the estimation of the inclusions' properties.

Following this method, a table correlating the percentage of CNTs (with E_{CNT}= 470 GPa) with the composites E can be created. This methodology may be used for creating properties tables for any composites of any number of materials and any number of inclusion geometric shapes. The Finite Element – random orientation tensor method approximation proved the more accurate, being closer to experimental data.

6.2 Optimization algorithm

According to the presented optimization methodology, the volume fraction required to attain a target effective modulus was successfully calculated with great accuracy. The success of the present procedure is demonstrated in Figs 6a and 6b. Every point of the diagrams represents an optimization case with a specific maximum number of iterations. As depicted in Fig. 6a the calculated effective modulus approximates the target effective modulus when the cycles of the optimization are close to 1000. In case convergence is achieved after the competition of 200 up to 1000 cycles, the accuracy of the calculated homogenized modulus is more than 99,9 %. Additionally, the CNTs volume fraction approaches the experimental volume fraction in case the optimization has 1000 maximum iterations. A Cost-Effectiveness analysis comparing the various composite combinations is easily performed. In conclusion, the method presented is a reliable approach that may be applied to identify the optimal percentage of reinforcement in a matrix, even with composites containing inclusions of different shape, form and material.

Bibliography

1. *Introduction to the compositeand its toughening mechanisms.* Qin, H. s.l. : Australian National University, Acton, ACT, Australia, 2015, Vol. Toughening mechanisms in composite materials.

2. https://firenzecolor.com/product/silver-mica-flakes/.

3. *Research Progress on Applications of Polyaniline (PANI) for Electrochemical Energy Storage and Conversion.* Qin, Li Gong. 3, s.l. : Materials, 2020, Vol. 13. 548.

4. https://www.123rf.com.

5. *https://www.quora.com/Whats-the-difference-between-aramid-fiber-and-carbon-fiber.*

6. *Building construction: The invention of reinforced concrete.* Encyclopedia Britannica.

7. *The First Reinforced-Concrete Skyscraper: The Ingalls Building in Cincinnati and Its Place in Structural History.* Condit, Carl W. 1, 1968, Technology and Culture, Vol. 9, pp. 1–33. doi:10.2307/3102041. JSTOR 3102041..

8. *History of Concrete.* S, Richard W. s.l. : www.theconcreteproducer.com, 1955.

9. *Reinforced Concrete.* Morgan, W. s.l. : www.jfccivilengineer.com, 1995, Vol. The Elements of Structure.

10. *History of Concrete Building Construction.* s.l. : Department of Civil Engineering , CIVL 1101, University of Memphis, 2015.

11. *Biographical Dictionary of the History of Technology.* Lance Day, Ian McNeil. s.l. : Routledge, 1996. ISBN 9780415193993.

12. *Concrete-steel Construction: (Der Eisenbetonbau).* Mörsch, Emil. 1909, The Engineering News Publishing Company, pp. 204-210.

13. *https://en.wikipedia.org/wiki/Joseph_Monier.*

14. *Concrete: The Vision of a New Architecture.* Collins, Peter. s.l. : McGill-Queen's University Press, 1920–1981, pp. 58–60. ISBN 0-7735-2564-5..

15. *Episode 81: Rebar and the Alvord Lake Bridge.* Mars, Roman. 2014, 99% Invisible.

16. *Concrete: The Vision of a New Architecture.* Collins, Peter. s.l. : McGill-Queen's University Press, pp. 61-64. ISBN 0-7735-2564-5..

17. *https://medium.com/anne-t-kent-california-room-community-newsletter/ernest-l-ransome-the-engineer-who-put-the-steel-in-concrete-2e127e371f07.* Anne T. Kent, California Room.

18. *Los Angeles from the Mountains to the Sea.* McGroarty, John Steven. s.l. : Los Angeles, CA: American Historical Society, 1921, p. 176.

19. *Annual Report of the City Auditor.* City of Los Angeles, California for the Year Ending June 30. Los Angeles, CA: Los Angeles City Auditor : s.n., 1905, pp. 71-73.

20. *What Builders are Doing.* Williams, D. 1907, Carpentry and Building, Vol. 66.

21. *Reinforced Concrete Buildings at Los Angeles, Ca.* W.P.H. 449, 1906, Letters to the Editor. Engineering News-Record, Vol. 55.

22. *Partial Collapse of the Bixby Hotel at Long Beach.* Austin, J. C., et al., et al. 1, 1906, Architect and Engineer of California, Vol. 7. 44-48.

23. *Julia Morgan-designed Mills bell tower counts down to its 115th anniversary.* Callan, Will. s.l. : https://hoodline.com/2019/02, 2019.

24. s.l. : https://swsu.ru/sbornik-statey/pdf/08_chapter%201.pdf.

25. *Horse Hair in your walls? Maybe so...* Dominick, Ned. s.l. : http://neddominicktheinspector.blogspot.com/2012/02.

26. *J.-M. Bonard, N.H. Thomson, A.J. Kulik, L. Forró, W. Benoit & L. Zuppiroli, Mechanical properties of carbon nanotubes.* Salvetat, J.-P. Applied Physics, Vol. A.

27. *Hong Guo, Chengchang Jia, Fazhang Yin, Ximin Zhang, Xuebing Liang & Hui ChenThermal Properties of Carbon Nanotube–Copper Composites for Thermal Management Applications.* Chu, Ke. Nanoscale Research Letters.

28. *, Emad Omrani, Pradeep L Menezes, Pradeep K RohatgiMechanical and tribological properties of self-lubricating metal matrix nanocomposites reinforced by carbon nanotubes (CNTs) and graphene – A review.* Moghadam, Afsaneh Dorri.

29. *Q. Wang & V. K. Varadan, Mechanical properties of carbon nanotube/polymer composites.* Arash, B.

30. *S. H. Pezzin, S. C. Amico, C. P. Bergmann & L. A. F. Coelho, The matrix stiffness role on tensile and thermal properties of carbon nanotubes/epoxy composites.* Loos, M. R.

31. *The reinforcement role of carbon nanotubes in epoxy composites with different matrix stiffness.* LijieCiJinBoBai. 3–4, March 2006, Composites Science and Technology, Vol. 66, pp. Pages 599-603.

32. *Über die Beziehung zwischen den beiden Elastizitäts konstanten isotroper Körper.* Voigt, W. 1889, Wied. Ann., Vol. 38, pp. 573-587.

33. *Berechnung der Fließgrenze von Mischkristallen auf Grund der Plastizitäts bedingung für Einkristalle.* Reuss, A. 1929, Z.angew. Math.Mech, Vol. 9, pp. 49-58.

34. *The Determination of the Elastic Field of an Ellipsoidal Inclusion,and Related Problems.* Eshelby, J.D. London : s.n., 1957. Proc.R.Soc.LondonA,241(1226),pp.376–396.doi: 10.1098/rspa.1957.0133. Vol. A.

35. *Tanaka K, Average Stress in the Matrix and Average Elastic Energy of Materials with Misfitting Inclusions.* T., Mori. 21, 1973, Acta Metall., pp. 571–574.

36. *Rosen, B.W., The Elastic Moduli of Fiber-Reinforced Materials.* Hashin, Z. 1964, J. Applied Mech., Vol. 3, pp. 223-232.

37. *Lo, K.H., Solutions for Effective Shear Properties in Three-phase Sphere and Cylinder Models.* Christensen, R. 1979, J. Mech. Phys. Solids, Vol. 27, pp. 315-330.

38. Chang (Karen) Yan, Thesis. *ON HOMOGENIZATION AND DE-HOMOGENIZATION OF COMPOSITE MATERIALS.* s.l. : Drexel University, November 2003.

39. *Development of an RVE and its stiffness predictions based on mathematical homogenization theory for short fibre composites, .* C.S.Upadhyay, K.P.Babu P.M.Mohite. January 2018, , International Journal of Solids and Structures,, Vols. Volumes 130–131,, pp. Pages 80-104.

40. *2. Study of the Effectiveness of the RVEs for Random Short Fiber Reinforced Elastomer Composites.* Lili Chen, Boqin Gu, Jianfeng Zhou, and Jiahui Tao,. , No.7, , 2019, , Fibers and Polymers , Vol. Vol.20, pp. 1467-1479.

41. *3. Homogenization of random heterogeneous media with inclusions of arbitrary shape modeled by XFEM,.* Dimitris Savvas, George Stefanou , Manolis Papadrakakis , George Deodatis, ,. 2014, Comput Mech.

42. *The sequential addition and migration method to generate representative volume elements for the homogenization of short fiber reinforced plastics,.* Schneider, Matti. ,2017), , Computational Mechanics, Vol. volume 59, pp. pages247–263(.

43. Yang, C.C. *Effect of the transition zone on the elastic Moduli of mortar.* Keelung, Taiwan, Republic of China : Institute of Materials Engineering, National Taiwan Ocean University, Pergamon, 1998.

44. *R. Kryvoruk, Meso-scale analysis of FRC using a two-step homogenization approach.* Gal, E. 89, 2011, Computers & Structures, Vol. 11, pp. 921-929.

45. *A critical evaluation for a class of micromechanics model.* RM, Christensen. 1990, J Mech Phys Solids, Vol. 38, pp. 39–404.

46. *E. Suday, H.Waisman, Homogenization of materials having inclusions surrounded by layers modeled by the extended finite element method.* Gal, E. 3, 2013, Journal for Multiscale Computational Engineering, Vol. 11, pp. 239–252.

47. *Multiscale simulation of mechanical properties and microstructure of CNT-reinforced cement-based composites,.* J.F. Wang, L.W. Zhang, K.M. Liew,. (2017), Comput. Methods Appl. Mech. Engrg., Vol. 319 , pp. 393–413.

48. *X. Liu, Y. Yuan, H. Mang, Multiscale modeling of the effect of the interfacial transition zone on the modulus of elasticity of fiber-reinforced fine concrete.* Zhang, J. 55, 2015, Computational Mechanics, Vol. 1, pp. 37-55.

49. Qsymah, A. *Sharma, R, Yang, J, Margetts, L & Mummery, P, Micro X-ray computed tomography image-based two-scale homogenisation of ultra high performance fibre reinforced concrete.* s.l. : Elsevier, 2016.09.020.

50. S., Metaxa Z. *Mechanical Behaviour and Durability of advanced cement based materials, Ph.D Thesis.* 2012.

51. *Highly Dispersed Carbon Nano-tube Reinforced Cement Based Materials.* Metaxa, Z.S., Shah, S.P., et al. 2010, Cement and Concrete Research, Vol. 40, pp. 1052-1059.

52. *Carbon Nanotubes Reinforced Concrete.* Z. S. Metaxa, S. P. Shah, et al. SP-267-2, ACI Special Publication on Nanotechnology of Concrete: The Next Big Thing is Small, pp. 11-20.

53. *Oleg Lourie, Mark J. Dyer, Katerina Moloni, Thomas F. Kelly, Rodney S. Ruoff, Strength and Breaking Mechanism of Multiwalled Carbon Nanotubes Under Tensile Load.* Yu, Min-Feng. Jan 2000, Science.

54. *Mills College: Julia Morgan.* Campanil, El. 1903-1904.

55. *Julia Morgan-designed Mills bell tower counts down to its 115th anniversary.* Callen, Will. s.l. : hoodline.com, 2019.

56. *Bay Area Architect Julia Morgan's Legacy Wasn't Just Hearst Castle.* Littman, Julie. s.l. : busnow.com, 2018.

57. *How one building survived the San Francisco earthquake and changed the world.* Olsen, Erik. s.l. : California Science Weekly, 2020.

58. Materials, Standard Specifications for Portland Cement of the American Society for Testing. s.l. : Standard No. 1. Philadelphia, PA: National Association of Cement Users, 1906.

59. Concrete, Standard Building Regulations for the Use of Reinforced. s.l. : Philadelphia, PA: National Association of Cement Users, 1910.

60. *Improvement in adhesion of cellulose fibers to the thermoplastic starch matrix by plasma treatment modification.* Fazeli, Mahyar, Florez, Jennifer Paola and Simão, Renata Antoun. 163, s.l. : Composites Part B: Engineering, 2019, pp. 207-216. doi:10.1016/j.comp.

61. *Smart Composites: Mechanics and Design.* Elhajjar, Rani, La Saponara, Valeria and Muliana, Anastasia. s.l. : Composite Materials, CRC Press. ISBN 978-1-138-07551-1.

62. *https://www.fabheads.in/blogs/the-age-of-composite-materials-history-classification-applications/.*

63. *Composites Manufacturing.* Mazumdar, Sanjay K. 2002, Composites Manufacturing, Materials, Product and Process Engineering.

64. *Impact of New Materials on Basic Manufacturing Industries—Case Study: Composite Automobile Structure.* P, Beardmore, C.F. Johnson, and G.G. Strosberg, Ford Motor Co. 1987.

65. *The Use of Polymer Composites in Construction.* Humphreys, M. F. s.l. : Queensland University Of Technology, Australia, 2003, Vol. Proceedings of the CIB 2003 Int'l conference on Smart and Sustainable Built Environment, pp. 1-9.

66. *Applications of composites in marine industry.* S.Ilaiyavel. s.l. : Journal of Engineering Research and Studies, 2011.

67. https://www.mar-bal.com/language/en/applications/history-of-composites/.

68. *Seismic Response of a Hybrid Fiber-Reinforced Concrete Bridge Column Detailed for Accelerated Bridge Construction.* Wilson Nguyen, William Trono, Marios Panagiotou, Claudia P. Ostertag. s.l. : PEER Report 2014/19 Pacific Earthquake Engineering Research Center Headquarters at the University of California, Berkeley, Vol. PEER Report 2014/19.

69. *COMPOSITE IN AEROSPACE MANUFACTURING INDUSTRY.* Sayuti, M. s.l. : Mini Project during PhD, at , 2016.

70. Foshan Hexbond Building Materials Co., Ltd. s.l. : http://www.hongzan.net/html/Products/Rockwool_Composite_Materials/2012/1127.

71. *Statistical analysis for freeze–thaw resistance of cement mortars containing marble dust and glass fiber.* Oğuzhan Keleştemur, Servet Yildiz, Bihter Gökçer, Erdinç Arici. s.l. : Elsevier,Materials & Design, 2014, Vol. 60, pp. 548-555.

72. *The Key Players in the Global Ceramic Matrix Composites (CMC).* ASDReports.com / ASDMedia BV - Veemkade 356 - 1019HD Amsterdam - The Netherland : https://www.asdreports.com/news-5633/key-players-global-ceramic-matrix-composites-cmc, 2015.

73. *Prediction of the cyclic durability of woven-hybrid composites.* Marya Raji, Hind Abdellaoui, HamidEssabir, Charles-AmaniKakou, RachidBouhfid, Abou el kacem Qaiss. s.l. : ScienceDirect, 2019, Composites Science and Engineering, pp. 27-62. https://doi.org/10.1016/B978-0-08-102290-0.00003-9.

74. https://simulatemore.mscsoftware.com/lightweight-high-performance-composites-what-is-a-composite-material/. 2013.

75. https://www.hindawi.com/journals/ijps/2020/8834518/.

76. https://deadliestwarrior.fandom.com/wiki/Mongol_Composite_Bow.

77. *History of Egyptian Masks.* s.l. : http://www.historyofmasks.net/mask-history/, 2021.

78. *Leo Hendrick Baekeland and the Invention of Bakelite.* s.l. : American Chemical Society, Students& Educators, Explore Chemistry, Chemical Landmarks, Bakelite: First Synthetic Plastic. https://www.acs.org/content/acs/en/education/whatischemistry/landmarks/bakelite.html.

79. *A Dome History Snapshot: The Radome.* s.l. : The Farley Group, 2016, Vols. Air-Structure News And Updates. https://www.thefarleygroup.com/blogs/a-dome-history-snapshot-the-radome.htm.

80. *Damage mechanisms in pultruded unidirectional fiberreinforced composites under static and fatigue loads.* Vergani, L. Dipartimento di Meccanica, Politecnico di Milano, Italy : WIT Transactions on State of the Art in Science and Engineering, Vol. 21. ISSN 1755-8336.

81. ANSYS. *manual.*

82. Swanson, Gabriel J. DeSalvo and John A. *ANSYS Engineering Analysis System User's Manual.* Houston, Pa : Swanson Analysis Systems, 1985.

83. *A critical evaluation for a class of micromechanics model.* Christensen, RM. 1990, J Mech Phys Solids, Vol. 38, pp. 39–404.

84. *Über die Beziehung zwischen den beiden Elastizitäts konstanten isotroper Körper.* Voigt, W. s.l. : Wied. Ann, 1889, Vol. vol. 38, pp. pp. 573-587.

85. *Berechnung der Fließgrenze von Mischkristallen auf Grund der Plastizitäts bedingung für Einkristalle.* Reuss, A. 1929, Z.angew. Math.Mech, Vol. vol. 9, pp. pp. 49-58.

86. *Average Stress in the Matrix and Average Elastic Energy of Materials with Misfitting Inclusions.* T Mori., K Tanaka. 1973, Acta Metall, Vol. vol. 21, pp. pp. 571–574.

87. *Multiscale homogenization method for the prediction of elastic properties of fiber-reinforced composites.* Wenya Shu, Ilinca Stanciulescu. v. 203, s.l. : Elsevier, 2020, International Journal of Solids and Structures, pp. pp. 249-263.

88. *Evaluation of effective material properties of randomly distributed short cylindrical fiber composites using a numerical homogenization technique.* Harald Berger, Sreedhar Kari, Ulrich Gabbert, Reinaldo Rodríguez Ramos, Julian Bravo Castillero and Raúl Guinovart Díaz. v. 2, No. 8, s.l. : mathematical sciences publishers, 2007, Journal of Mechanics of Materials and Structures, pp. pp. 1561-1570. 10.2140/jomms.2007.2.1561.

89. *Modeling of the effect of particles size, particles distribution and particles number on mechanical properties of polymer-clay nano-composites: Numerical homogenization versus experimental results.* Y Djebara, A El Moumen, T Kanit, S Madani, A Imad. s.l. : Elsevier, 2016, Composites Part B: Engineering, Vol. v.86, pp. pp. 135-142. https://doi.org/10.1016/j.compositesb.2015.09.034.

90. Abaqus, Documentation. 2017, https://abaqus-docs.mit.edu/2017/English/SIMACAEMATRefMap/simamat-c-meanfieldhomogenization.htm.

91. *A homogenization scheme for elastoplastic composites using concept of Mori-Tanaka method and average deformation power rate density.* Zengrui Song, Xianghe Penga, Shan Tang, Tao Fua. s.l. : Elsevier, 2020, International Journal of Plasticity, Vol. v. 125. https://doi.org/10.1016/j.ijplas.2019.102652.